NASA CR-111811

INVESTIGATION MONITORING AND CONTROL OF LARGE TELESCOPE PERFORMANCE

BY DR. KENT E. ERICKSON

PREPARED UNDER CONTRACT NASW-1856

KEUFFEL & ESSER COMPANY
MORRISTOWN, NEW JERSEY

NATIONAL AERONAUTICS & SPACE ADMINISTRATION

WASHINGTON, D.C.

SEPTEMBER 1970

FOREWORD

The purpose of this contract is to provide the National Aeronautics and Space Administration with research relating to the monitoring and control of large telescope performance in general accordance with Keuffel & Esser Company proposal dated April 15, 1966, as revised September 27, 1968.

This is a feasibility study using a laser interferometer and zone-plate combination to monitor the optical performance of large telescopic systems. It is directed toward the following:

a) to determine the minimum efficiency required of the zone plate.

b) to test the performance of the laser interferometer when used with light diffracted from the zone plate.

c) to further the technology of generating very large zone plates.

The control aspect of the original proposal was not included in this contract.

TABLE OF CONTENTS

ABSTRACT ---------- 1

SYMBOLS---------- 3

1. DESCRIPTION OF THE ZONE PATTERN MONITORING TECHNIQUE

1.1 Basic Monitoring Technique

1.1.1 Dependence on Zone Location

1.1.2 Automated Sensing and Interpretation

1.2 Application to the Secondary Mirror

1.3 Nature of the Zone Pattern

1.4 Generating Techniques for the Zone Pattern

1.5 Calibration Procedures

TABLE OF CONTENTS (Cont'd.)

2. ANALYTICAL STUDY

2.1 Effect of Diffraction on Stellar Images

2.1.1 Effect on Image Resolution

2.1.2 Effect on Image Intensity

2.1.3 Effect on Background Brightness

2.1.3.1 Radiation from a Single Star

2.1.3.2 Galactic Radiation

2.1.3.3 Solar Radiation

2.2 Tolerance Analysis of the Zones

2.2.1 General Relations

2.2.2 Strain Effects

2.2.3 Fringecounter Measurement Tolerances for Direct Calibration

2.3 Signal Power at the Sensors

2.4 Appendices

2.4.1 Diffraction Analysis

2.4.2 Aberration Analysis of a Holographically Generated Zone Pattern

TABLE OF CONTENTS (Cont'd.)

3. EXPERIMENTAL STUDY

3.1 Telescope/Interferometer System

3.1.1 Telescope

3.1.2 Interferometer

3.2 Generation of the Zone Pattern

3.2.1 Holographic Arrangement

3.2.2 Photosensitive Material

3.2.3 Dipcoater

3.2.4 Photographic Procedure

3.2.5 Results

3.3 Performance of the Monitor

3.3.1 Adjustment Characteristics

3.3.2 Intensity Characteristics

4. CONCLUSIONS

ILLUSTRATIONS

Figure No.	Drawings	Page No.
1	Telescope Monitoring and Control Schematic	6
2	Diffraction at the Monitoring Wave	10
3	Diffraction Loss from Type "A" Zones	19
4	Diffraction Loss from Type "B" Zones	21
5	Minimum Sub-zone Width and Total Number of Zones	23
6	Holographic Zone Pattern Generation	29
7	(Deleted)	
8	Calibration Method "A"	33
9	Diffraction from Type "A" Zones	120
10	Diffraction from Type "B" Zones	126
11	Zone Geometry	134
12	Telescope and Monitor	158
14	Interferometer	164
18	Holographic Zone Plate Generator	180

ILLUSTRATIONS (Cont'd.)

Figure No.	Photographs	Page No.
13	Telescope and Monitor	161
15	Interferometer	167
16	Holographic Arrangement (Looking Toward the Mirror)	175
17	Holographic Arrangement (Looking Toward the Laser)	177
19	Beamsplitter	183
20	Dipcoater	189
21	Zone Pattem(7" Diameter)	203
22	Zone Pattern (10" Diameter)	205
23	Vertical Tilt	217
24	Horizontal Tilt	219
25	Defocused (Inward)	221
26	Defocused (Outward)	223
27	Optimum Focus	225
28	Distortion	227
29	Fringe Quality at an Attenuation of .36%	231
30	Fringe Quality at an Attenuation of .0031%	233

ABSTRACT

In the monitoring technique investigated herein, a laser interferometer is located at the focal plane of the telescope. A zone pattern, very lightly imprinted on the primary mirror, diffracts a small portion of the light back to the interferometer for monitoring purposes. The resulting interference pattern contains information on the total performance of the primary mirror (figure, alignment and focus) as used in the telescope.

It was originally proposed that the most suitable method of generating a very large zone pattern (e.g. 3m in diameter) would be to scribe it with an interferometrically controlled ruling engine using a laser "stylus". Funding limitations dictated, however, that a holographically generated zone plate must suffice for this feasibility study.

The major effort, therefore, went into holographically producing a satisfactory zone pattern. Ultimately a zone pattern of unexpectedly good quality was attained. This pattern was etched into the surface of an f/5, 12" diameter primary mirror in a cassegranian telescope.

It was of particular interest to determine whether the proposed monitoring method could employ a zone pattern so weak as not to interfere significantly with normal operation of the telescope. This study indicates that diffraction loss from the zone plate could be kept below 3% and that the background from diffracted light should not obscure stars brighter than approximately magnitude 28.

SYMBOLS

A = Wave Amplitude

a, b, c, d (Section 2.4.2 only) (See Figure 11, P. 134)

a = Zone Period

B = Brightness

b = Width of each half-zone for 1st order diffraction

D = Diameter of the primary mirror

F = Focal length of the primary mirror

$f = \frac{F}{D}$ = Aperture ratio of the primary mirror

$f_r = \frac{F}{2r}$ = Aperture ratio at a zone of radius

g, h (See p. 141)

I = Irradiance

M = Zone number

N = Order of diffraction for the monitoring light

N' = Order of diffraction for starlight

R = Radius of curvature of the primary mirror

r = Zone radius (See Figure 1, p. 10)

T = Temperature of the mirror

t = Step height of the zones

U (See p. 147)

v (See p. 137)

W (See p. 147)

x, y = Cartesian coordinates on the mirror surface

SYMBOLS (Cont'd.)

α_o = Coefficient of thermal expansion

α (See Figure 11, p. 134)

β (See Figure 11, p. 134)

β' = Diffraction angle

δ_o (See p. 137)

δ = Mirror surface deformation

ϵ_λ = Fraction of starlight diffracted out of order zero

ϵ_N = Fraction of the monitoring light diffracted into order N

ηb = Width of the narrower subzone (See Figure 4, p. 21)

γ_r (See p. 11)

$\gamma = \lambda / \lambda_o$

λ_o = Wavelength of the monitoring light

λ = Wavelength of starlight

ϕ (See Figure 10, p. 126)

ϕ (Section 2.4.2 only) (See Figure 11, p. 134)

ρ (See p. 151)

θ (See Figure 10, p. 126)

θ (Section 2.2.2 only) = polar coordinate on the mirror

Ω = Solid angle

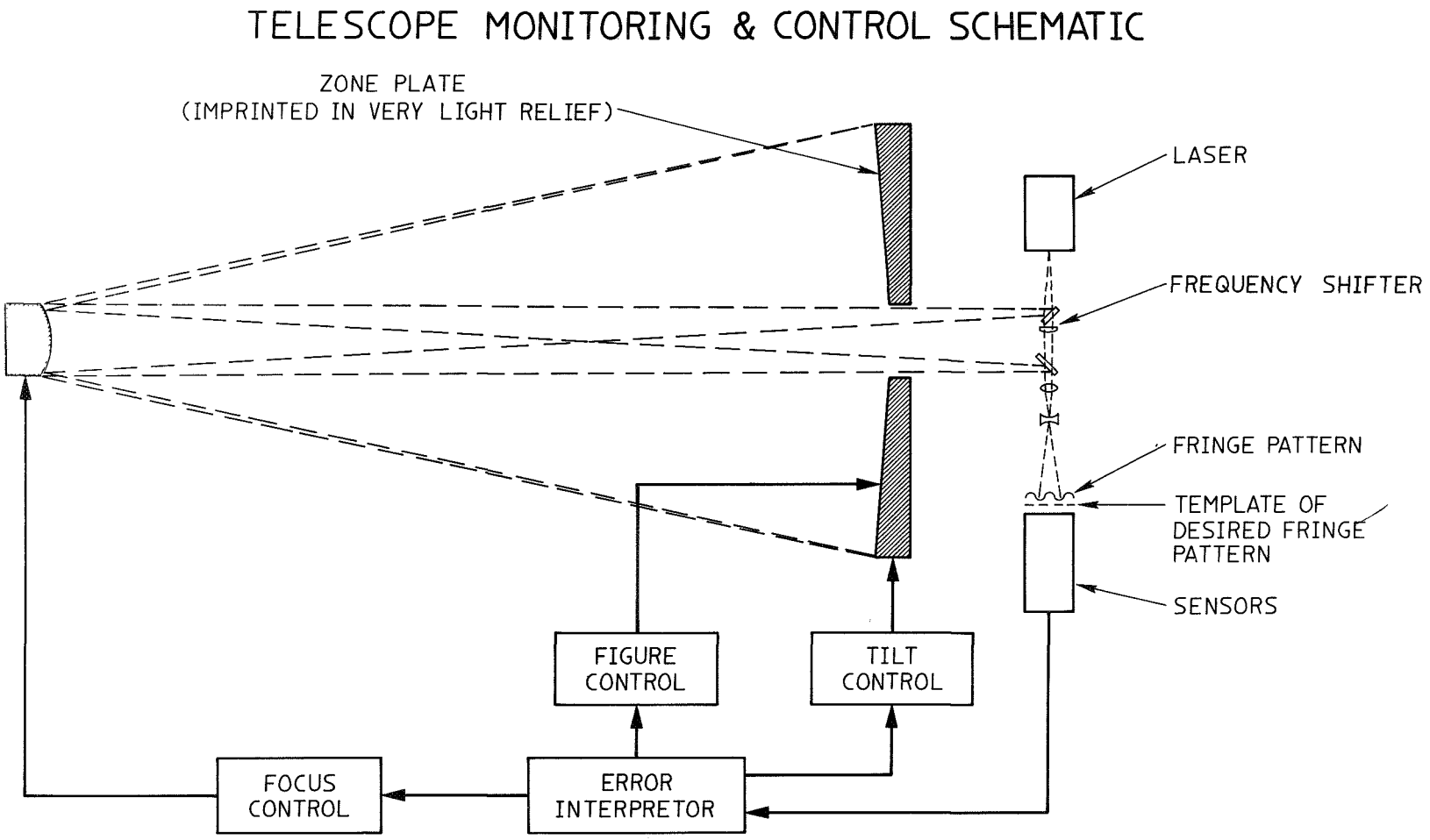
TELESCOPE MONITORING & CONTROL SCHEMATIC
ZONE PLATE
(IMPRINTED IN VERY LIGHT RELIEF)
LASER
FREQUENCY SHIFTER
FRINGE PATTERN
TEMPLATE OF
DESIRED FRINGE
PATTERN
SENSORS
FIGURE
CONTROL
TILT
CONTROL
FOCUS
CONTROL
ERROR
INTERPRETOR

FIGURE 1

1. DESCRIPTION OF THE ZONE PATTERN MONITORING TECHNIQUE

1.1 Basic Monitoring Technique

In monitoring the performance of a very large telescope, it is desirable that the monitoring light traverse the optical system as nearly as possible in the same way as starlight. The total performance of the primary mirror as used in the telescope can then be evaluated.

In the technique under investigation here, the monitor is located at the focal plane of the telescope. The monitoring light passes through the telescope twice, once in the direction of starlight and once in the reverse direction.

The technique is illustrated in Figure 1. An interferometer with a laser source is located at the focal plane of the telescope. The laser emits a uniphase wavefront which is divided into a "monitoring wave" and a "reference wave". The "monitoring wave" passes through the telescope. A small fraction is diffracted from the zone pattern on the primary mirror, and returns to the interferometer.

Interference between the returning "measuring wave" and the "reference wave" generates a fringe pattern across the image of the primary mirror.

DIFFRACTION OF THE MONITORING WAVE

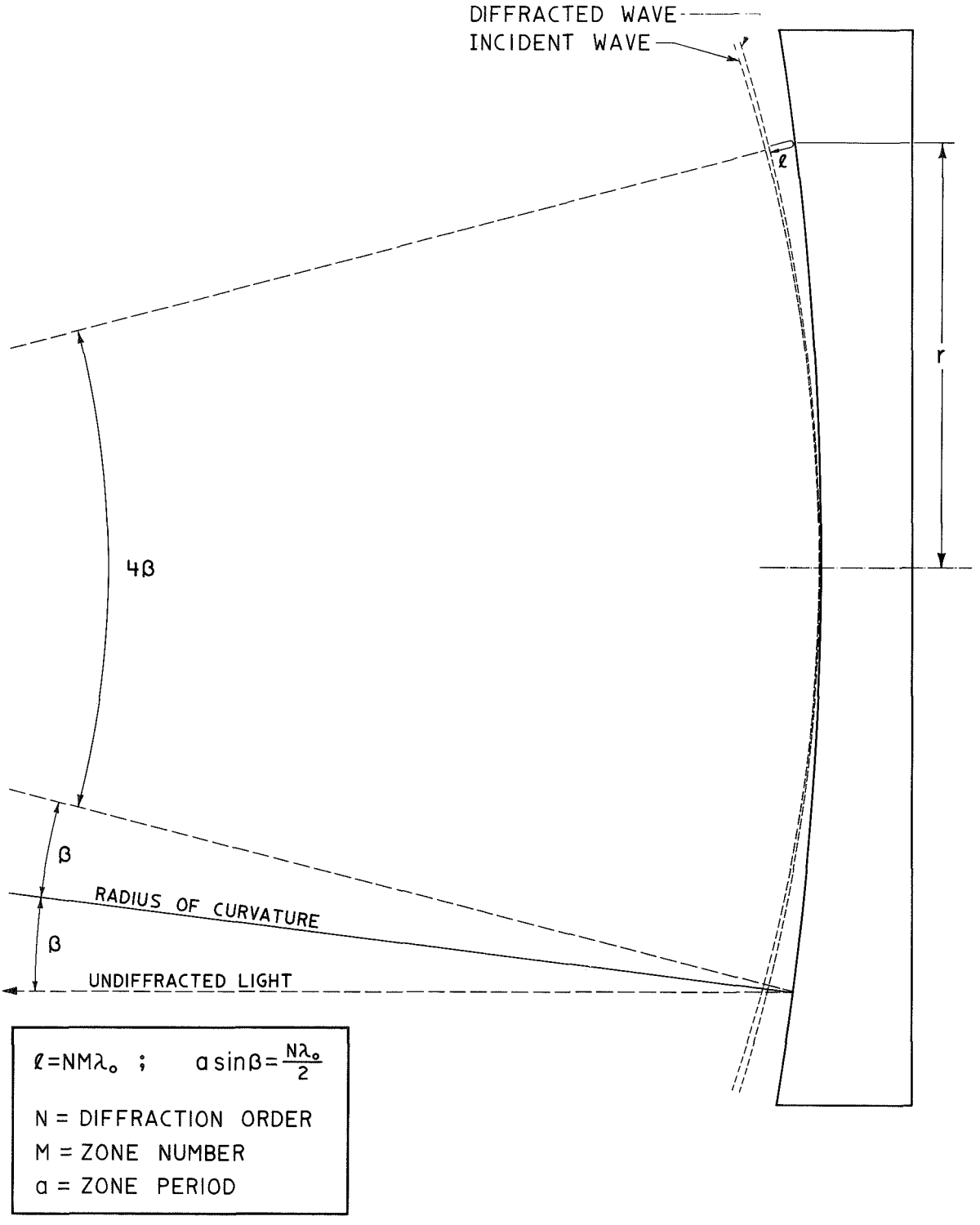

$\ell = NM\lambda_o$; $a \sin\beta = \frac{N\lambda_o}{2}$

N = DIFFRACTION ORDER
M = ZONE NUMBER
a = ZONE PERIOD

FIGURE 2

This fringe pattern is compared with a template of the pattern which corresponds to perfect figure, focus, and alignment of the primary mirror with respect to the secondary mirror.

1.1.1 Dependence on Zone Location

As illustrated in Figure 2 , the shape of the diffracted wavefront depends upon the zone pattern. For Nth order diffraction, the path difference, ℓ, between the incident and the diffracted wavefronts at the Mth zone is exactly $NM\lambda_o$.

Fortunately, an error Δr in the radial location of the zones has much less influence on the shape of the diffracted wavefront than does an equal displacement Δz in the surface of the mirror. The sensitivity ratio, γ, is given by:

$$\gamma_r = \frac{1}{4 f_r} \qquad (1)$$

where, f_r = aperture ratio of the mirror at the zone in question. For example, if $f_r = 4$, an error in zone location of $\frac{\lambda_o}{8}$ (i.e., standard fringecounter resolution) would introduce an error into the monitor of only $\frac{\lambda_o}{128}$.

Ideally, it is desirable that the zones be located so that a spherical returning wavefront corresponds to perfect figure of the mirror. The fringes in

the monitor then ought to be straight and parallel. Practically, however, this is not necessary. As long as the interference pattern which corresponds to perfect performance of the mirror is known, deviations from this pattern can be interpreted in a straightforward manner.

1.1.2 Automated Sensing and Interpretation

In the present investigation, the interference pattern was recorded photographically. For use with a control system, it would, of course, be necessary to use photodetectors.

Figure 1 shows how automatic sensing might be done. A frequency shifter in the reference beam causes the fringes to sweep across the template of the desired fringe pattern. An array of detectors is located behind the template. When the fringe pattern matches the desired pattern, the signals are all in phase. When the two patterns do not match, the differences result in phase differences, ϕ_{ij} , in the electrical signals.

These phase differences, ϕ_{ij} , from the detector array must be analyzed to determine errors in tilt, focus and surface figure of the mirror. The error in tilt about any given axis is represented essentially by the first moment of the ϕ_{ij} about that axis. The error in focus is represented essentially by the polar moment of the ϕ_{ij} about the centroid. What remains after these errors are removed represents residual error in the surface figure of the mirror.

1.2 Application to the Secondary Mirror

Since the secondary mirror is double-passed whereas the primary mirror is not, whatever error is present in the figure or alignment of the secondary mirror is not compensated. A second interferometer could be set up to monitor the performance of the secondary mirror by means of a similar zone pattern lightly imprinted on its surface.

During the initial checkout, a secondary monitor would be highly desirable since a large convex surface is extremely difficult to check by other means. After checkout, the secondary interferometer and zone pattern might be removed; the figure of the secondary mirror is not likely to change and alignment and focus of the secondary mirror with respect to the focal point of the telescope are not as critical.

1.3 Nature of the Zone Pattern

The zone pattern is in low relief and overcoated to give uniform reflectivity. In modern terminology, this is a "reflection phase hologram".

The zones are circular and spaced so as to give an essentially spherical shape to the diffracted wavefront. This results in the following condition for the zone period, a :

$$a \approx 2N f_r \lambda_o \qquad (2)$$

Almost any practical means of generating the zones will yield an essentially "square wave" profile. There are then two methods of limiting the diffraction efficiency of the zones so that they do not interfere appreciably with normal operation of the telescope:

A. Limiting the step height, t , of the zones.

B. Limiting the number of zones and the width of each raised (or lowered) sub-zone.

The resulting zones are herein referred to as type "A" and type "B" respectively.

Zone profiles of type "A" and type "B" are illustrated in Figures 3 & 4. In type "A" zones, each sub-zone has a width $b = \frac{a}{2}$. In type "B" zones, the period, a , is increased by a factor of N while the width of the narrower sub-zone is reduced by a factor of η .

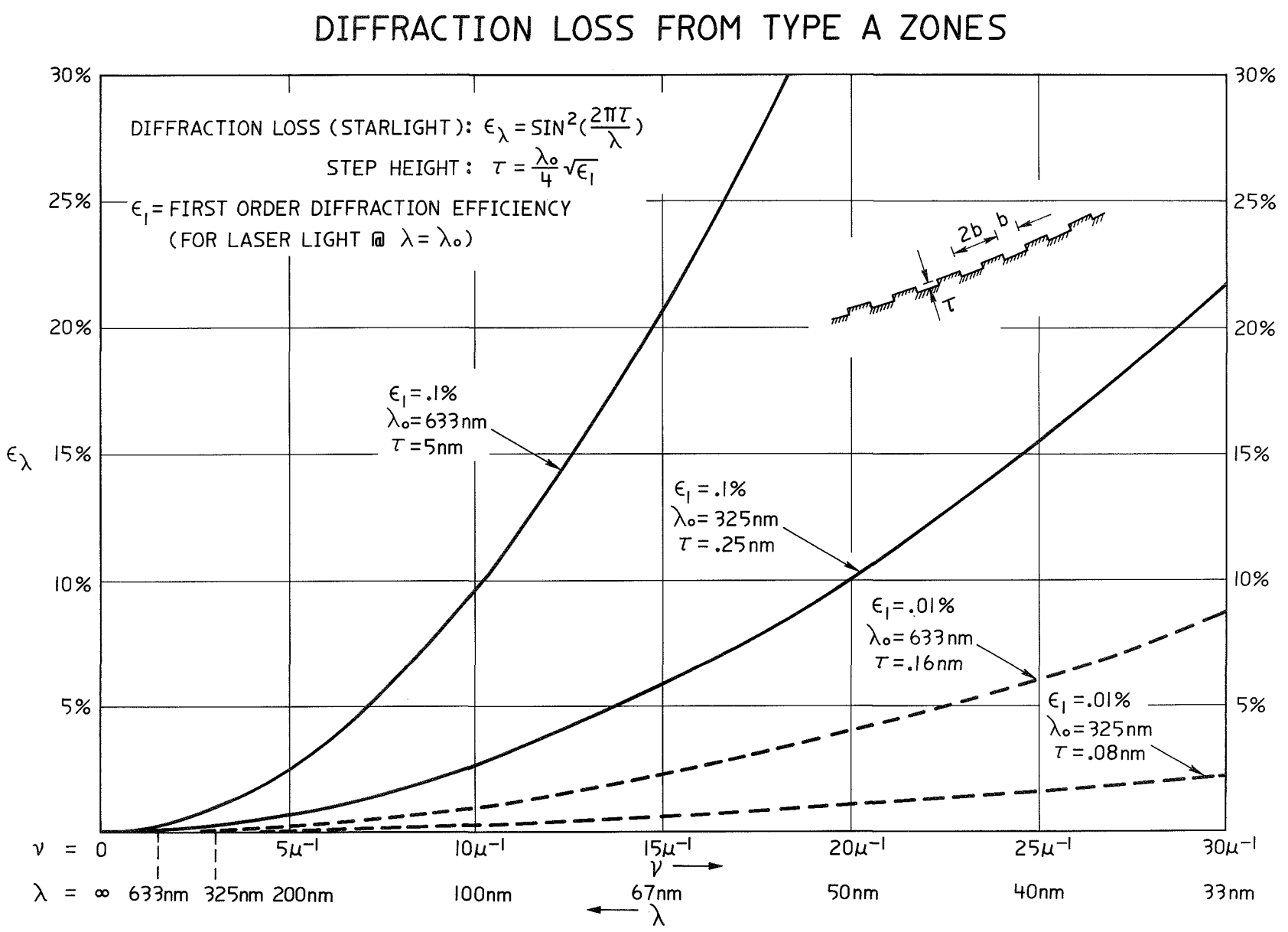
DIFFRACTION LOSS FROM TYPE A ZONES
DIFFRACTION LOSS (STARLIGHT): $\epsilon_\lambda = \sin^2(\frac{2\pi\tau}{\lambda})$
STEP HEIGHT: $\tau = \frac{\lambda_o}{4}\sqrt{\epsilon_1}$
ϵ_1 = FIRST ORDER DIFFRACTION EFFICIENCY
(FOR LASER LIGHT @ $\lambda = \lambda_o$)
2b
b
τ
ϵ_1 = .1%
λ_o = 633nm
τ = 5nm
ϵ_1 = .1%
λ_o = 325nm
τ = .25nm
ϵ_1 = .01%
λ_o = 633nm
τ = .16nm
ϵ_1 = .01%
λ_o = 325nm
τ = .08nm
ϵ_λ
30%
25%
20%
15%
10%
5%
ν = 0
$5\mu^{-1}$
$10\mu^{-1}$
$15\mu^{-1}$
$20\mu^{-1}$
$25\mu^{-1}$
$30\mu^{-1}$
ν
λ = ∞
633nm
325nm
200nm
100nm
67nm
50nm
40nm
33nm
λ

FIGURE 3

DIFFRACTION LOSS FROM TYPE B ZONES

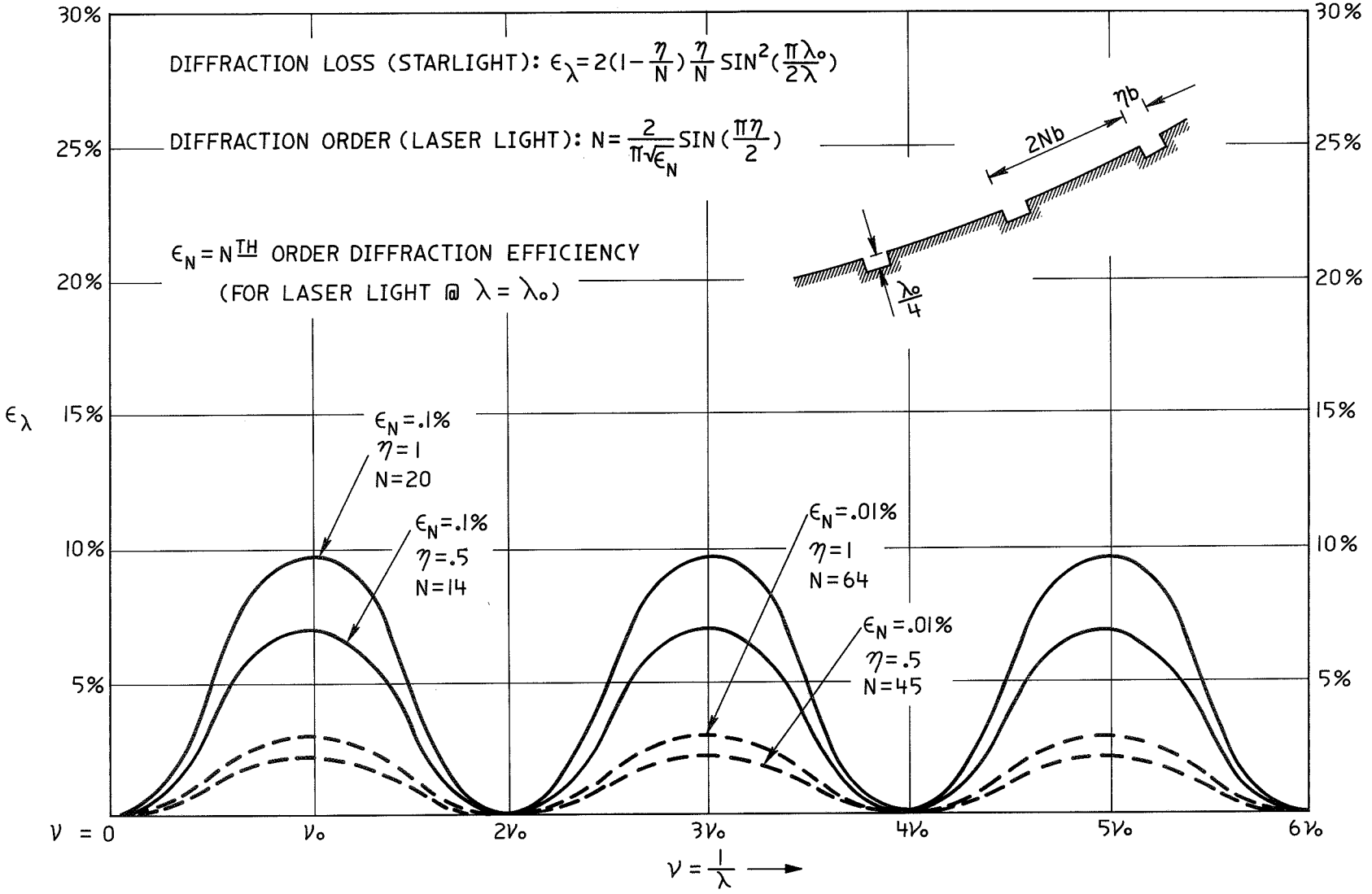

FIGURE 4

MINIMUM SUB-ZONE WIDTH AND TOTAL NUMBER OF ZONES

CALCULATED FOR AN f/4 MIRROR OF DIAMETER D=3m

MINIMUM SUB-ZONE WIDTH $[b_{(min)}=\eta\lambda_o f]$			
η \ λ_o	633nm	442nm	325nm
.75	1.8μm	1.3μm	1.0μm
1.0	2.5μm	1.8μm	1.3μm

TOTAL NUMBER OF ZONES $[M=\frac{D}{8N\lambda_o f}]$			
N \ λ_o	633nm	442nm	325nm
1	148,000	212,000	289,000
14	10,600	15,100	20,600
20	7,400	10,600	14,400
45	3,300	4,700	6,400
64	2,300	3,300	4,500

FIGURE 5

The narrowest zones occur at the periphery of the mirror. The width of the narrowest sub-zone is tabulated in Figure 5 for various values of λ_o & η. The total number of zones (neglecting obscuration by the secondary mirror) is also tabulated for various values of λ_o & N.

It is not necessary that the zone pattern cover the entire reflective face of the primary mirror. Instead, the pattern might cover only those areas imaged onto the detector array, plus enough connective corridors to establish continuity of the fringes. Alternatively, the spacing of the array might simply be made small enough that uniformity of the mirror surface could be relied upon to establish continuity of the fringes. The pattern would then reduce to an array of isolated areas.

1.4 Generating Techniques for the Zone Pattern

There are two basic approaches to generating the zone pattern:

A. The pattern may be generated holographically using interference between two laser beams. (See Figure 6)

B. The pattern may be scribed into the mirror coating using an interferometrically controlled "laser stylus". (See Figure 7)

It is doubtful that the holographic approach is feasible for a 3m mirror. The scale of the holographic setup would be enormous and even if holography were possible (despite atmospheric and seismic disturbances), the resultant pattern would almost certainly require independent calibration. Furthermore, the variety of zone profiles which can be generated holographically is limited.

The scribing technique, on the other hand, while undoubtedly costly, appears entirely feasible. Moreover, it offers the prospect that all high precision measurements necessary for checkout of the telescope can be made on the primary mirror alone before it is installed in the telescope. Furthermore, during measurement of the zones, the figure of the mirror need not be precisely controlled.

HOLOGRAPHIC ZONE PATTERN GENERATION

IDEAL GEOMETRY

Two coherent sources; wavelength λ_0

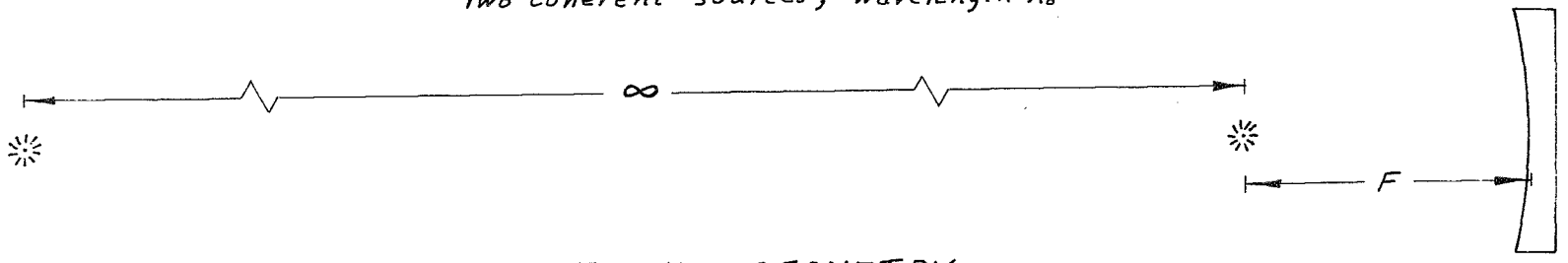

COMPROMISE GEOMETRY

Two coherent sources; wavelength $\lambda < \lambda_0$

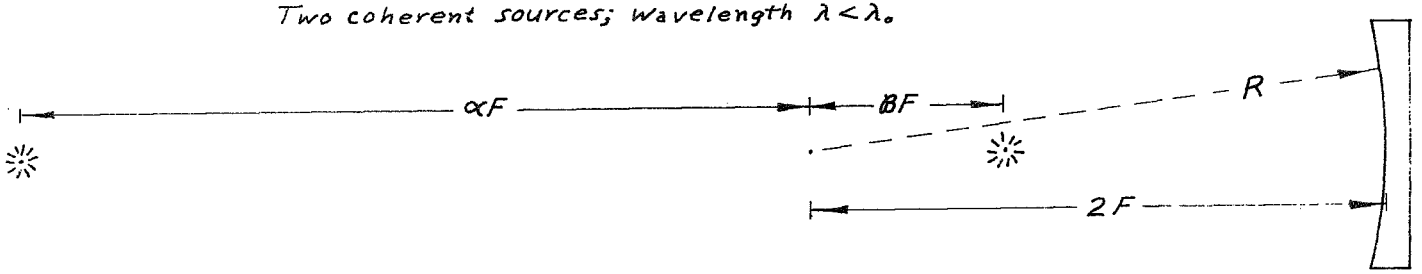

$$\alpha = \frac{4\gamma^2 - \gamma - 2 + \sqrt{4 - 3\gamma^2}}{2\gamma(1-\gamma)} \qquad \beta = \frac{4\gamma^2 + \gamma - 2 + \sqrt{4 - 3\gamma^2}}{2\gamma(1+\gamma)} \qquad \left[\gamma \equiv \frac{\lambda}{\lambda_0}\right]$$

FIGURE 6

1.5 Calibration Procedures

The fringe pattern which corresponds to perfect figure, focus, and alignment of the primary mirror with respect to the secondary mirror must be established. Two methods are possible:

A. For calibration, the figure of the primary mirror may be monitored by an auxiliary interferometer at the center of curvature and the alignment and focus may also be monitored by independent means. (See Figure 8)

B. The zone pattern may be generated (or mapped) to high accuracy using a specially designed, fringecounter controlled "circular ruling engine" with a "laser stylus". The fringe pattern which corresponds to perfect performance of the primary mirror can then be calculated using the design parameters of the telescope plus test results on the optical performance of the interferometer and the secondary mirror.

Contrary perhaps to initial appearances, method "B" should be more accurate than method "A". Provided the zone locations are accurately known, the relationship between the incident and the diffracted wavefronts is just as well defined for the Nth order diffraction used in method "B" as for the zero order diffraction used (at the center of curvature) in method "A". Any error in the figure of the secondary mirror enters identically (except for sign) in both cases.

CALIBRATION METHOD "A"

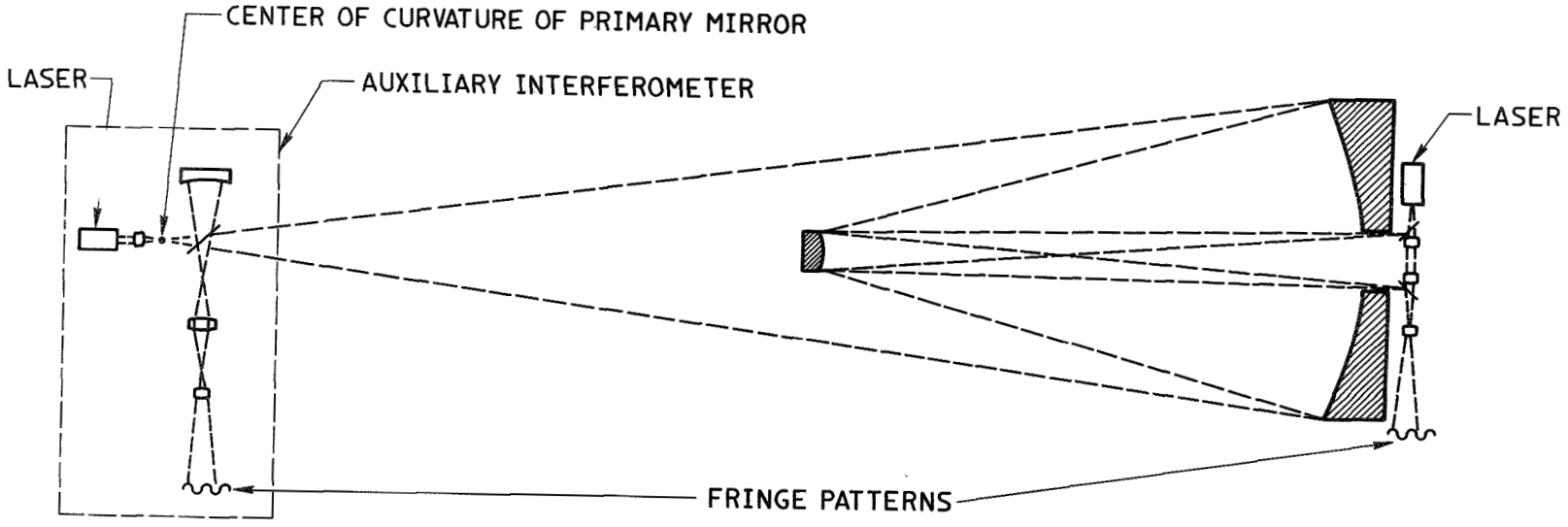

FIGURE 8

In method "A", however, two fringe patterns must be measured and compared. Errors in measurement and errors from atmosphere and seismic disturbances contribute to the total error budget. In method "B", on the other hand, precision measurements are required only on the individual components, not on the assembled telescope. Furthermore, the figure of the primary mirror need not be controlled precisely during measurement of the zones.

Neither method of calibration can set the focus with final accuracy. The focus of the telescope must, therefore, be readjusted in orbit to optimize stellar images. The focus of the interferometer must also be readjusted so that the fringe pattern in the monitor may remain unchanged.

It should be noted that method "A" is not applicable to a secondary monitor which might be used to monitor the performance of a convex secondary mirror.

2. ANALYTICAL STUDY

2.1 Effect of Diffraction on Stellar Images

For the zone pattern method to be practical, it must be possible to use a zone pattern which is so faint as to have no substantial adverse effect on the performance of the telescope. In this connection, there are three principal questions to be answered:

1. What is the effect on image quality? (i.e.: How does the zone pattern affect the distribution of light in the stellar image?)
2. What is the effect on image intensity? (i.e.: How much light does the zone pattern diffract out of the stellar image?)
3. What is the effect on background intensity? (i.e.: How much does the light diffracted by the zone pattern contribute to the background intensity?)

2.1.1 Effect on Image Resolution

2.1.1.1 Type "A" Zones

As shown in Figure 9 , the zone height, t , will affect the phase and amplitude of the zero order light. For all practical values of t , the phase shift will be well below $\frac{\pi}{10}$ and the intensity change well below 10% for all wavelengths $\lambda > 100$ nm. Furthermore, these effects are essentially the same for all zones. Therefore, provided the zone pattern is uniform, the resolution will be essentially unaffected (except insofar as diffracted light would tend to obscure very faint stars (see section 2.1.3).)

If the zone pattern were to be applied only to certain portions of the mirror (e.g., discrete annuli) the phase and amplitude of the light would not be uniformly affected over the surface of the mirror. In the far U.V. ($\lambda < 100$ nm) these nonuniformities might then become large enough that their effect on image quality would no longer be negligible.

2.1.1.2 Type "B" Zones

As shown in Figure 10, the narrow sub-zones of width ηb and height t will affect the phase ϕ and amplitude A_0 of the zero order light. The

net effect, however, over an entire zone of width $2Nb$ is very small. For all practical choices of N and η, the phase shift will be well under 2° and the intensity change well below 10%. Furthermore, these effects are essentially the same for all zones. Except insofar as diffracted light would tend to obscure very faint stars (see section 2.1.3), the resolution would be essentially unaffected.

2.1.2 Effect on Image Intensity

The amount of starlight diffracted out of the stellar image depends upon several factors:

1. The diffraction efficiency (ϵ_1 or ϵ_N) for the monitoring laser light.
2. The wavelength, λ , of the starlight.
3. The nature of the zone pattern.

The diffraction losses from type "A" and "B" zones are analyzed in section 2.4.1. These losses are plotted in Figures 3 and 4 as a function of λ for various values of ϵ_1 or ϵ_N and other parameters. It is assumed in Figures 3 and 4 that the zone pattern covers the entire surface of the mirror. If the pattern covers only a fraction of the mirror surface, the net diffraction loss will be proportionately reduced.

2.1.2.1 Type "A" Zones

In type "A" zones the diffraction efficiency is kept low by keeping the step height of the zones small. As the wavelength, λ , of the starlight decreases, however, the step height, t , becomes more significant and diffraction losses increase. The disadvantage of type "A" zones for any telescope which must work in the far U.V. is obvious from Figure 3 .

Stellar diffraction losses can be reduced by reducing the step height, t, but a limit is eventually reached where the diffraction efficiency, ϵ_1, becomes insufficient for monitoring purposes. On the other hand, the diffraction efficiency, ϵ_1, improves as the wavelength λ_o of the monitoring light is reduced.

2.1.2.2 Type "B" Zones

In type "B" zones, the diffraction efficiency is kept low by increasing the diffraction order N for the monitoring light. The zone period is N-fold greater than that for type "A" zones. The width of the narrower region in each zone, however, is kept at a value ηb not far different from the half-width b for type "A" zones. The step height is set at $\frac{\lambda_o}{4}$ to give maximum diffraction efficiency at the monitoring wavelength λ_o. (See Figure 4).

Diffraction losses for starlight can be cut by increasing the diffraction order N or by decreasing the width factor η until a limit is reached where the diffraction efficiency ϵ_N becomes insufficient for monitoring purposes. As far as the net diffraction loss, ϵ_λ, for starlight is concerned, decreasing the width factor, η, has much the same effect as increasing the diffraction order, N. However, as far as the diffraction efficiency, ϵ_N, for the monitoring light is concerned, it is somewhat more efficient to decrease η than to increase N, especially if $\eta > \frac{1}{2}$.

Because they diffract proportionately more light into the higher orders, type "B" zones diffract somewhat more starlight in the neighborhood of the monitoring wavelength, λ_o, than do type "A" zones. The performance of type "B" zones in the far U.V. region, however, is much superior.

2.1.3 Effect on Background Brightness*

Starlight diffracted out of each zero order image will contribute to the brightness of the background. We consider here two distinct cases:

A. The effect of a single bright star within (or close to) the field of view.

B. The average effect from large numbers of lesser stars in the galactic plane.

In addition, we consider solar radiation although this is highly dependent upon telescope geometry and baffeling.

---

*We use the term "brightness" to mean radiant power per unit area per unit solid angle whether or not it is visible. We use the term "irradiance" to mean radiant power per unit area whether or not it is visible.

2.1.3.1 Radiation from a Single Star

Starlight diffracted out of order N = 0 forms images in orders $N \neq 0$. These images are out of focus in the focal plane of the telescope.

The maximum diffraction angle for the Nth diffraction order is given by:

$$\theta_{N'} \approx \frac{N' \lambda}{2 N f \lambda_0} \qquad (3)$$

Except for obscuration by the secondary mirror, the diffracted Nth order light thus uniformly fills a solid angle $\Omega_{N'}$ in the field of view given by:

$$\Omega_{N'} = \pi \theta_{N'}^2 \qquad (4)$$

We ignore obscuration by the secondary mirror and utilize the fact that the diffracted light is uniformly bright over the aperture of the primary mirror. The spectral brightness (brightness per unit of spectral bandwidth) of the Nth diffraction order is thus given by:

$$B_{N'}(\lambda) = \frac{\epsilon_{N'} I_\lambda}{\Omega_{N'}} \qquad (5)$$

where:

I_λ = Spectral irradiance (irradiance per unit of spectral bandwidth) of the star at the primary mirror.

$\epsilon_{N'}$ = Fraction of I_λ diffracted into order N'.

Substitution of (3) and (4) into (5) gives:

$$B_{N'}(\lambda) = \frac{\epsilon_{N'}(\lambda)\, I_\lambda}{\pi} \left(\frac{2 N f \lambda_0}{N' \lambda} \right)^2 \qquad (6)$$

From (96) of Section 2.4.1.2 we have:

$$\epsilon_{N'}(\lambda) = \left[\frac{2}{\pi N'} \sin\frac{\theta}{2} \sin\frac{\phi}{2} \right]^2 \qquad (7)$$

where:

$$\theta = \pi \eta \frac{N'}{N}$$

$$\phi = \frac{4\pi r}{\lambda}$$

The spectral brightness, B_λ , for all diffraction orders (except N = 0) combined is:

$$B_\lambda = \sum_{N'=1}^{\infty} B_{N'}(\lambda) \qquad (8)$$

Substitution of (6) and (7) into (8) gives:

$$B_\lambda \approx \frac{I_\lambda}{\pi} \sum_{N'=1}^{\infty} \left[\frac{4 N f \lambda_0}{\pi (N')^2 \lambda} \sin\left(\frac{\pi \eta N'}{2N} \right) \sin\frac{\phi}{2} \right]^2 \qquad (9)$$

2.1.3.1.1 Type "B" Zones

For type "B" zones:

$$N >> 1 \quad ; \quad \eta \leq 1 \; ; \quad \phi = \frac{\pi \lambda_c}{\lambda}$$

Because of the $\frac{1}{(N')^2}$ factor, the first few terms of (9) dominate.

For these terms the following approximation may be used:

$$\sin\left(\frac{\eta \pi N'}{2N}\right) \approx \left(\frac{\eta \pi N'}{2N}\right)$$

Hence, (9) becomes:

$$B_\lambda \approx \frac{I_\lambda}{\pi} \sum_{N'=1}^{\infty} \left[\frac{2\eta f \lambda_0}{N' \lambda} \sin\left(\frac{\pi \lambda_c}{2\lambda}\right)\right]^2$$

$$\approx \frac{\sqrt{2}\, I_\lambda}{\pi} \left[\frac{2\eta f \lambda_0}{\lambda} \sin\left(\frac{\pi \lambda_0}{2\lambda}\right)\right]^2$$

We wish to arrive at an estimate of the total background brightness, B.

This is given by:

$$B = \int B_\lambda d\lambda \approx \int \frac{\sqrt{2}\, I_\lambda}{\pi} \left(\frac{2\eta f \lambda_0}{\lambda}\right)^2 \sin^2\left(\frac{\pi \lambda_0}{2\lambda}\right) d\lambda \qquad (10)$$

The value of this integral depends upon the spectral characteristics of the star. We may obtain a general approximation by assigning an effective value of 1/2 to the oscillating $\sin^2\left(\frac{\pi \lambda_0}{2\lambda}\right)$ term and defining the following effective quantities:

$\tilde{\lambda}$ = effective wavelength of the star

$\mathcal{I}$ = effective total irradiance of the star upon the primary mirror

Thus (10) becomes:

$$B \approx \frac{2\sqrt{2}}{\pi}\left(\frac{\eta f \lambda_0}{\bar{\lambda}}\right)^2 I \qquad (11)$$

A very faint star in the neighborhood of the bright star will tend to be obscured by light diffracted out of the image of the bright star.

The light diffracted into the solid angle subtended by the faint star has an irradiance, I', at the primary mirror given by:

$$I' = B\,\Omega' \qquad (12)$$

where:

Ω' = solid angle subtended by the image of the faint star.

For most stars this solid angle is essentially that subtended by the airy diffraction disc. Thus:

$$\Omega' \approx \pi\left(\frac{1.22\,\bar{\lambda}'}{D}\right)^2 \qquad (13)$$

where:

$\bar{\lambda}'$ = effective wavelength of the faint star.

Substitution of (11) and (13) into (12) gives:

$$I' \approx 2\sqrt{2}\left(\frac{1.22\,\eta f \lambda_0 \bar{\lambda}'}{D\,\bar{\lambda}}\right)^2 I \qquad (14)$$

In terms of stellar magnitudes (14) may be written thus:

$$M' \approx M - 2.5 \log\left[2\sqrt{2}\left(\frac{1.22\eta f \lambda_c \bar{\lambda}'}{D\,\bar{\lambda}}\right)^{-2}\right]$$

$$M' \approx M + 5 \log\left[\frac{.490\,\bar{\lambda}}{\eta f \lambda_c \bar{\lambda}'}\right] \qquad (15)$$

where:

M' = Magnitude of the light diffracted from the bright star into the cone angle subtended by the airy disc of the faint star.

M = Magnitude of the bright star.

$\bar{\lambda}$ = Effective wavelength of the bright star.

$\bar{\lambda}'$ = Effective wavelength of the faint star.

A bright bluish star will have more tendency to obscure a faint reddish star than a bright reddish star will have to obscure a faint bluish star.

If we assume the following values:

$$\bar{\lambda}' = 2\bar{\lambda}$$
$$\lambda_c = .63\ \mu m$$
$$\eta = .75$$
$$f = 4$$
$$D = 3\ m$$

then:

$$M' \approx M + 28 \qquad (16)$$

This result indicates that light from a star of magnitude M = 0 diffracted by a type "B" zone pattern covering the entire primary mirror would obscure stars in its vicinity which are fainter than approximately magnitude 28.

2.1.3.1.2 Type "A" Zones

For type "A" zones:

$$N = 1 \; ; \; \eta = 1 \; ; \; \phi = \frac{2\pi t}{\lambda}$$

Hence, (9) becomes:

$$B_\lambda = \frac{I_\lambda}{\pi} \sum_{N'=1}^{\infty} \left[\frac{4 f \lambda_c}{\pi (N')^2 \lambda} \sin\left(\frac{\pi N'}{2}\right) \sin\left(\frac{2\pi t}{\lambda}\right) \right]^2 \quad (17)$$

Because of the $\sin^2\left(\frac{\pi N'}{2}\right)$ factor, all even orders are absent.

Because of this and the $\left(\frac{1}{N'}\right)^2$ factor, the first term of (17)

dominates. Thus:

$$B_\lambda \approx \frac{I_\lambda}{\pi} \left(\frac{4\pi \lambda_c}{\pi \lambda}\right)^2 \sin^2\left(\frac{2\pi t}{\lambda}\right) \quad (18)$$

The total background brightness, B, is given by:

$$B = \int B_\lambda \, d\lambda \approx \frac{1}{\pi} \int I_\lambda \left(\frac{4 f \lambda_c}{\pi \lambda}\right)^2 \sin^2\left(\frac{2\pi t}{\lambda}\right) d\lambda \quad (19)$$

How rapidly the $\sin^2\left(\frac{2\pi t}{\lambda}\right)$ term rises in the U.V. depends upon the step height t . Because of the severe wavelength dependence of (19), it is not possible to arrive at a generally accurate approximation. However, for all practical choices of t and for all useful values of λ , it is most probable that:

$$\sin^2\left(\frac{2\pi t}{\lambda}\right) < .1$$

Comparison of (19) with (10) (where we take $\eta = .75$; $\sin^2\left(\frac{\pi \lambda_c}{2\lambda}\right) = \frac{1}{2}$) shows that:

$$B_{(\text{Type "A" zones})} < .1 \; B_{(\text{Type "B" zones})} \quad (20)$$

Modification of (16) in accordance with (20) gives:

$$M' > M + 28 - 2.5 \text{ Log}[.1]$$

Thus, for type "A" zones:

$$M' > M + 30.5 \qquad (21)$$

The lower background produced by type "A" zones in the vicinity of a bright star is due to the fact that the average diffraction angle is greater than for type "B" zones. This also results in better shielding by the telescope barrel. In order for any light from a star to be diffracted in the direction of the telescope focus, the star must lie at an angle θ to the telescope axis such that

$$\theta > \frac{\lambda d}{2\lambda_0 F} \qquad (22)$$

where:

d = diameter of the secondary mirror.

F = focal length of the primary mirror.

The telescope barrel will thus shield a portion of the primary mirror having a maximum width of at least $\frac{\lambda d}{2\lambda_0}$. This will further reduce the apparent intensity of the diffracted light.

2.1.3.2 Galactic Radiation

The out-of-focus diffraction images from large numbers of individual stars in the vicinity of the field of view will produce a background whose brightness, B, is given by:

$$B = \int \epsilon_\lambda \, B_\lambda \, d\lambda \tag{23}$$

where:

B_λ = average spectral sky brightness in the vicinity of the field of view.

ϵ_λ = diffraction efficiency for all orders combined (except N = 0).

As an approximation, we again use effective values:

$\overline{\epsilon}$ = effective diffraction efficiency for all orders combined ($N \neq 0$).

$\overline{B}$ = effective sky brightness in the vicinity of the field of view.

thus:

$$B \approx \overline{\epsilon} \; \overline{B} \tag{24}$$

The galactic light diffracted into the solid angle, Ω', subtended by the star image thus has an irradiance, I', at the primary mirror of:

$$I' \approx \overline{\epsilon} \, \overline{B} \, \Omega' \tag{25}$$

Again we represent Ω' by equation (13):

$$\Omega' \approx \pi \left(\frac{1.22\bar{\lambda}'}{D}\right)^2 \tag{13}$$

thus:

$$I' \approx \pi \bar{\epsilon}\, \bar{B} \left(\frac{1.22\bar{\lambda}'}{D}\right)^2 \tag{26}$$

In terms of stellar magnitudes, (26) may be reexpressed thus:

$$M' = M_B + 2.5 \text{ Log} \left[\pi \bar{\epsilon} \left(\frac{D}{1.22\bar{\lambda}'}\right)^2\right] \tag{27}$$

where:

M' = magnitude of the galactic light diffracted into solid angle Ω' subtended by the star image.

M_B = magnitude per unit solid angle for galactic radiation.

It should be noted that almost all fainter stars have images whose resolution is limited only by diffraction from the primary mirror. The image brightness of such stars increases with the mirror diameter D whereas the brightness of scattered light does not. Therefore, as indicated by (26) and (27), the relative importance of scattered light decreases as D increases.

2.1.3.2.1 Type "B" Zones

ϵ_λ for type "B" zones is plotted in Figure 4 . For any practical choice of parameters we may assume that:

$$\epsilon < .03$$

In the galactic plane the maximum sky brightness in any $5^o \times 5^o$ solid angle is:*

$$M_B > -4 \quad \text{visual magnitudes/steradian}$$

If we choose,

$$\bar{\lambda}' = .5\,\mu m$$
$$D = 3\,m$$

Then substitution of the above values in (27) gives:

$$M' > 32 \tag{28}$$

This result indicates that if light from the brightest region of our galaxy were diffracted by a type "B" zone pattern covering the entire mirror, it would tend to obscure stars which are fainter than magnitude 32.

---

* Convenience tables of Outside Atmosphere Sky Brightness by Allen G. Bender and Robert E. Wilson, March 1969. NASA Document X-732-69-96.

2.1.3.2.2 Type "A" Zones

ϵ_λ for type "A" zones is plotted in Figure 3 . As in section 2.1.3.1.2 we assume that, for any practical choice of t and for all useful values of λ , it is probable that:

$$\bar{\epsilon}_\lambda < .1$$

If in (27) we use the same values for M_θ, $\bar{\lambda}'$ and D as in the previous section, then,

$$M' > 29.5 \qquad (29)$$

Comparison of (29) with (28) shows that type "A" zones diffract more galactic light than do type "B" zones.

2.1.3.2.3 Scatter from Irregularities

The foregoing analysis is for a perfectly regular zone pattern on a perfectly regular mirror. There will also be scatter due to irregularities in the zones and in the figure of the mirror. The magnitude of such scattering is hard to predict but as it has very little coherence it is not likely to exceed that of coherent scattering (i.e., diffraction).

2.1.3.3 Solar Radiation

2.1.3.3.1 Direct Illumination

The irradiance from the sun is roughly 10^{11} times that of starlight. Even the best baffling, therefore, would not prevent scattered sunlight from being the limiting factor if any substantial amount were to enter the telescope barrel. Observations on any given weak star must therefore be made at a time of year when sunlight will not strike surfaces interior to the telescope barrel.

2.1.3.3.2 Moonlight

The interior of the telescope barrel should be blackened and baffled so that once-reflected radiation cannot reach the primary mirror directly. Twice-reflected radiation will reach the primary mirror via second surfaces. We denote the entirety of such surfaces by "S".

We let:

ω = Average solid angle subtended by "S" as viewed from points directly illuminated by moonlight.

ω' = Average solid angle subtended by "S" as viewed from points on the primary mirror.

ρ' = Average reflection coefficient of the baffles.

Neglecting light reflected more than twice, a very rough approximation to the attenuation factor γ' for moonlight reaching the primary mirror is:

$$\gamma' \approx (\rho')^2 \left(\frac{\omega}{\pi}\right)\left(\frac{\omega'}{\pi}\right)$$

ω' will be smaller than ω because "S" will lie largely toward the end of the barrel farthest from the primary mirror.

We assume:

$$\omega \approx .05 \text{ sterradian}$$

$$\omega' \approx .01 \text{ sterradian}$$

$$\rho' \approx .1$$

This gives:

$$\rho' \approx 5 \times 10^{-6}$$

Since the irradiance from moonlight is roughly 10^5 times that of starlight, this indicates that reflected moonlight can be reduced to about the level of starlight.

2.2 Tolerance Analysis of the Zones

The zone pattern method of monitoring telescope performance is practical only if radial dimensions on the mirror are highly stable. Questions of stability are examined in Section 2.2.1.

The most practical method of calibrating the monitor appears to be that of measuring the zone radii with a fringecounter. The accuracy requirements for this are analyzed in Section 2.2.3.

2.2.1 General Relations

A radial displacement of the zones by Δr has an effect on the fringe pattern equivalent to that produced by an axial deformation δ of the mirror of

$$\delta = \gamma_r \Delta r \tag{30}$$

The relaxation factor, γ_r, in the sensitivity to radial displacement relative to axial displacement is given by:

$$\boxed{\gamma_r \approx \frac{r}{2F} = \frac{1}{4 f_r}} \tag{31}$$

where:

f_r = aperture ratio of the mirror at the zone of radius r.

In terms of its effect on the fringe pattern in the monitor, a radial displacement, Δr, in the zones produces a shift ΔM in the pattern of the following number of fringes:

$$\boxed{\Delta M = \frac{r \Delta r}{F \lambda_o}} \tag{32}$$

Relation (31) may be derived from Figure 2. The diffraction relation is:

$$2a \sin \beta' = N \lambda_o \tag{33}$$

where:

$\mathcal{B}$ = diffraction angle

a = zone period

But:

$$\sin \mathcal{B}' \approx \mathcal{B}' \approx \frac{1}{4 f_r} \tag{34}$$

Hence:

$$a \approx 2 N f_r \lambda_0 \tag{35}$$

We consider a radial displacement, Δr, of the zones equal to one zone period. In this case,

$$\Delta r = a \tag{36}$$

This shifts the fringe pattern by N fringes. To produce an equivalent shift, the mirror surface must be displaced a distance ΔZ given by:

$$\delta = \frac{N \lambda_0}{2} \tag{37}$$

Combining (35), (36) and (37) gives a sensitivity ratio γ_r of:

$$\gamma_r = \frac{\delta}{\Delta r} \approx \frac{1}{4 f_r} \tag{38}$$

Equation (32) may be derived by noting that:

$$\Delta M = N \frac{\Delta r}{a} \tag{39}$$

Combining (31) and (35) with (39) yields (32).

2.2.2 Material Strain Effects

2.2.2.1 Uniform Temperature Change

Because the zones expand thermally, whereas the wavelength, λ_o, of the monitoring light does not, a uniform temperature increase, ΔT, of the mirror affects the curvature of the diffracted wavefront.

The radial expansion is given by:

$$\Delta r = \alpha_o r \Delta T \tag{40}$$

According to (32), this produces a fringe shift, ΔM, in the monitor given by:

$$\Delta M = \frac{r \Delta r}{F \lambda_o} \tag{32}$$

Substitution of (40) into (32) gives:

$$\Delta M = \frac{\alpha_o \Delta T r^2}{F \lambda_o} \tag{41}$$

The largest fringe shift occurs at the periphery where $r = \frac{D}{2}$:

$$|\Delta M|_{max} = \frac{D |\alpha_o \Delta T|}{4 f \lambda_o} \tag{42}$$

If, for example,

$$\alpha_o = 10^{-7}/^oC$$
$$D = 3\ m$$
$$f = 4$$
$$\lambda_o = .63\ \mu m$$

then, (43)

$$|\Delta M|_{max} = .03\ fringe \times |\Delta T|$$

The fringe shift in (41) represents a shift in focus. If the focus is monitored by independent means (e.g., by using stellar images) then this fringe shift may be ignored. If, however, a correction is desired, it follows from (43) that a temperature measurement to an accuracy of $\pm 1^{\circ}$C would correspond to an accuracy of .015 λ_o in the shape of the mirror.

2.2.2.2 Uniform Temperature Gradient

We assume a temperature variation, $T(x,y)$, which gives a total temperature change of ΔT across the mirror. Thus:

$$T = \frac{x}{D}\,\Delta T \tag{44}$$

The resultant thermal deformation is a function of internal stresses developed in the mirror. We shall assume as a worst case that there is no shear resistance to deformation along paths $x = x_0$ and $y = y_0$ from the coordinate axes to a given point (x_0, y_0) on the mirror.

The thermal shift $(\Delta x, \Delta y)$ of point (x_0, y_0) is thus:

$$\Delta x_0 = \int_0^{x_0} \alpha_0 T(x, y_0)\,dx = \frac{\alpha_0 \Delta T}{2D} x_0^2$$
$$\Delta y_0 = \int_0^{y_0} \alpha_0 T(x_0, y)\,dy = \frac{\alpha_0 \Delta T}{D} x_0 y_0 \tag{45}$$

The radial shift, Δr, in a zone of radius r passing through point (x_0, y_0) is given by:

$$\Delta r = (\Delta x_0)\cos\theta + (\Delta y_0)\sin\theta \tag{46}$$

In polar coordinates, r, θ :

$$x_0 = r\cos\theta$$
$$y_0 = r\sin\theta \tag{47}$$

Substituting (45) and (47) in (46) gives:

$$\Delta r = \frac{\alpha_0 \Delta T}{2D}\left[\cos^3\theta + 2\cos\theta\sin^2\theta\right] r^2 \tag{48}$$

According to (32), a zone shift, Δr, produces a fringe shift, ΔM, in the monitor given by:

$$\Delta M = \frac{r\,\Delta r}{f\,\lambda_0} \tag{32}$$

Thus:

$$\Delta M = \frac{\alpha_0 \Delta T}{2DF\lambda_0}\left[\cos^3\theta + 2\cos\theta\sin^2\theta\right] r^3 \tag{49}$$

The maximum fringe shift, $|\Delta M|_{max}$, occurs at $r = \frac{D}{2}$, $\cos\theta = \sqrt{\frac{2}{3}}$

Thus:

$$|\Delta M|_{max} = \frac{\sqrt{2}\, D\,|\alpha_0 \Delta T|}{36\, f\,\lambda_0} \tag{50}$$

If, for example, we choose:

$\alpha_0 = 10^{-7}/^{\circ}C$

$D = 3\ m$

$f = 4$

$\lambda_0 = .63\ \mu m$

then,

$$|\Delta M|_{max} = .005 \frac{\text{fringe}}{^{\circ}C} |\Delta T|$$

Much of the shift ΔM given by (49) is simply a tilt of the wavefront which does not affect the image quality. The effect of this tilt may be removed from (49) by subtracting a term linear in x to give a residual abberation $\Delta M'$:

$$\Delta M' = A\left[\cos^3\theta + 2\cos\theta\sin^2\theta\right] - C\, r\cos\theta \tag{51}$$

Where $A = \frac{\alpha_0 \Delta T}{2D^2 f \lambda_0}$ (52)

Neglecting obscuration by the secondary mirror, the r.m.s. fringe shift, $(\Delta M')_{rms}$, over the mirror surface is:

$$(\Delta M')_{rms} = \left[\frac{4}{\pi D^2}\int_0^{2\pi}\int_0^{\frac{D}{2}} (\Delta M')^2 r\,dr\,d\theta\right]^{\frac{1}{2}} \qquad (53)$$

Substitution of (51) into (53) and evaluation of the integral gives:

$$(\Delta M')_{rms} = \frac{D}{8}\left[\frac{13A^2D^4}{8} - 10AD^2C + 16C^2\right]^{\frac{1}{2}} \qquad (54)$$

The value of C which minimizes (54) is given by:

$$C = \frac{5}{16}AD^2 \qquad (55)$$

Substitution of (52) and (55) into (54) gives:

$$(\Delta M')_{rms} = \frac{D|\alpha_0 \Delta T|}{64 f d_0} \qquad (56)$$

If we again choose:

$$\alpha_0 = 10^{-7}/^{\circ}C$$
$$D = 3\ m$$
$$f = 4$$
$$\lambda_0 = .63\ \mu m$$

Then:

$$(\Delta M')_{rms} = .002\ \frac{\text{fringe}}{^{\circ}C}\,|\Delta T|$$

Under these conditions, it would require a temperature difference of $10^{\circ}C$ across the mirror in order to produce an effect on the monitor equivalent to a $\frac{\lambda}{100}$ r.m.s. deformation of the mirror figure.

2.2.2.3 Non-Uniform Temperature Gradient

We assume a saddle-shaped temperature variation $T(x,y)$ across the mirror such that at $x = \pm \frac{D}{2}$, $y = 0$ the temperature is higher by ΔT than it is at $x = 0$, $y = \pm \frac{D}{2}$:

$$T = \frac{2\Delta T}{D^2}(x^2 - y^2) \tag{57}$$

Again, we shall assume as a worst case that there is no shear resistance to deformation along paths $x = x_0$ & $y = y_0$ from the coordinate axes to a given point (x_0, y_0) on the mirror. The thermal shift, $(\Delta x_0, \Delta y_0)$, of a point (x_0, y_0) is thus:

$$\Delta x_0 = \int_0^{x_0} \alpha_0 T(x, y_0)\, dx = \frac{2\alpha_0 \Delta T}{3D^2}\left[x_0^3 - 3x_0 y_0^2\right]$$
$$\Delta y_0 = \int_0^{y_0} \alpha_0 T(x_0, y)\, dy = \frac{2\alpha_0 \Delta T}{3D^2}\left[3x_0^2 y_0 - y_0^3\right] \tag{58}$$

Substitution of (58) into (46) gives:

$$\Delta r = \frac{2\alpha_0 \Delta T}{3D^2}\left[\cos^4\theta - \sin^4\theta\right] r^3 \tag{59}$$

According to (32), a zone shift, Δr, produces a fringe shift, ΔM, in the monitor given by:

$$\Delta M = \frac{r\,\Delta r}{F\lambda_0} \tag{32}$$

Thus:

$$\Delta M = \frac{2\alpha_0 \Delta T}{3D^2 F\lambda}\left[\cos^4\theta - \sin^4\theta\right] r^4 \tag{60}$$

The maximum fringe shift, $|\Delta M|_{max}$, occurs at $r = \frac{D}{2}, \theta = 0$.

Thus:

$$|\Delta M|_{max} = \frac{D|\alpha_c \Delta T|}{24 f \lambda} \tag{61}$$

If, for example, we again choose:

$$\alpha_c = 10^{-7}/^{\circ}C$$
$$D = 3\ m$$
$$f = 4$$
$$\lambda_c = .63\ \mu m$$

then,

$$|\Delta M|_{max} = \frac{.005\ fringe}{^{\circ}C} \times |\Delta T| \tag{62}$$

Neglecting obscuration by the secondary mirror, the r.m.s. fringe shift, $(\Delta M)_{rms}$, over the mirror surface is:

$$(\Delta M)_{rms} = \left[\frac{4}{\pi D^2}\int_0^{2\pi}\int_0^{\frac{D}{2}} (\Delta M)^2 r\, dr\, d\theta\right]^{\frac{1}{2}} \tag{63}$$

Substitution of (60) into (62) and evaluation of the integral gives:

$$(\Delta M)_{rms} = \frac{\sqrt{2}\, D|\alpha_c \Delta T|}{64 f \lambda_o} \tag{64}$$

If we again choose:

$$\alpha_c = 10^{-7}/^{\circ}C$$
$$D = 3\ m$$
$$f = 4$$
$$\lambda_c = .63\ \mu m \tag{65}$$

then,

$$(\Delta M)_{rms} = .0026\ fringe/^{\circ}C\ |\Delta T|$$

Under these conditions, it would require a temperature difference of $\Delta T = 8^{\circ}C$ between points 90° apart on the periphery of the mirror in order to produce an effect on the monitor equivalent to a $\frac{\lambda_o}{100}$ r.m.s. deformation of the mirror figure.

2.2.2.4 Effect of Material Creepage

The tolerances set forth above for strain of thermal origin also apply to radial strain from creepage of the substrate. More experience is necessary with large blanks of materials such as "Cer-vit"(R), "Zerodur"(R) and "ULE Quartz"(R) before it will be known if their long term stability is adequate. "Cer-vit"(R) and "Zerodur"(R) are the better prospects since their strain birefringence values indicate that internal stresses (at least on a macroscopic scale) are normally much lower than those of "ULE Quartz"(R).

(R) "Cer-vit", "Zerodur" and "ULE Quartz" are registered trade names of materials supplied respectively by Owens-Illinois, Schott, and Corning.

2.2.3 Fringecounter Measurement Tolerances for Direct Calibration

If the monitor is calibrated by method (B) of section 1.5, the zone radii must be measured with a fringecounter. The major tolerance requirements are analyzed in the following sections.

2.2.3.1 Systematic Error

Since a fringecounter is an incremental measuring device whereas the zone radii must be measured absolutely, it is of interest to establish the absolute accuracy with which the fringecount must be preset.

According to (32), an error (Δr) in the zone radius has the same effect on the monitor as an error δ in mirror figure where δ is given by:

$$\delta = \frac{r \Delta r}{2F} \tag{66}$$

If Δr is constant over the entire mirror, the principal effect is simply to shift the focus by an amount ΔF. Since the focus will be adjusted in orbit to optimize stellar images, this focal shift is of no consequence.

We, therefore, define a new error function δ' in which the function $C r^2$ representing the mean focal shift has been removed:

$$\delta' = \frac{r \Delta r}{2F} - C r^2 \tag{67}$$

We define:

$$(\delta')_{rms} = \left[\frac{4}{\pi D^2} \int_0^{2\pi} \int_0^{\frac{D}{2}} (\delta')^2 r \, dr \, d\theta\right]^{\frac{1}{2}} \tag{68}$$

Substitution of (67) in (68) gives:

$$(\delta')_{rms} = \frac{D}{2}\left[\frac{(\Delta r)^2}{8F^2} - \frac{(\Delta r) DC}{5F} + \frac{D^2 C^2}{12}\right]^{\frac{1}{2}} \tag{69}$$

The value of c which minimizes (69) is:

$$c = \frac{6(\Delta r)}{5DF} \tag{70}$$

Substitution of (70) into (69) gives:

$$(\delta')_{rms} = \frac{\sqrt{2}(\Delta r)}{40} \tag{71}$$

If, for example, we assume that the fringecounter can be preset to an accuracy of ± 4 counts on a standard fringecounter (i.e. $\pm .32_{\mu m}$), then, for an f/4 mirror:

$$(\delta')_{rms} = \frac{\lambda}{180} \quad \text{at} \quad \lambda = 500\,nm$$

2.2.3.2 Roundoff Error

In a standard fringecounter, the roundoff error (Δr) is:

$$\Delta r = \pm \frac{\lambda}{8} \qquad @ \ \lambda = .63 \ \mu m$$

According to (66) the maximum effect of roundoff error occurs at $r = \frac{D}{2}$. This effect is equivalent to a mirror deformation $|\delta|_{max}$ given by:

$$|\delta|_{max} = \frac{|\Delta r|}{4F} \tag{72}$$

If we assume an f/4 mirror, then,

$$|\delta|_{max} = \frac{\lambda}{100} \qquad at \quad \lambda = 500 \ nm$$

Roundoff error can thus be ignored even though, in certain regions, it may not be random.

2.2.3.3 Random Error

We assume that the rms error, $(\Delta r)_{rms}$, in any annular region of the mirror is essentially independent of the radius. It then follows from (66) that:

$$(\delta)^2_{rms} = \frac{4}{\pi D^2}\int_0^{2\pi}\int_0^{\frac{D}{2}}\left[\frac{r(\Delta r)_{rms}}{2F}\right]^2 r\,dr\,d\theta$$

$$(\delta)_{rms} = \frac{\sqrt{2}}{8f}(\Delta r)_{rms} \qquad (73)$$

If, for example, we restrict $(\Delta r)_{rms}$ to two counts on a standard fringecounter (i.e., $.15\mu m$) then, for an f/4 mirror:

$$(\delta)_{rms} \leq \frac{\lambda}{75} \qquad @\ \lambda = 500\ nm$$

2.3 Signal Power at the Sensors

In a heterodyne detection system, the signal power, P_s, incident on a single detector in the array is:

$$P_s = 2\gamma_1\sqrt{P_r P_m} \tag{74}$$

where,

γ_1 = Fraction of the total mirror area imaged onto a single detector.

P_r = Power in the reference beam.

P_m = Power in the monitoring beam.

We define:

τ = Transmissivity of the beamsplitter.

P_o = Power emitted by the laser.

γ_2 = Loss factor from stops, etc.

Thus:

$$\begin{aligned} P_r &= \gamma_2\,\tau(1-\tau)\,P_o \\ P_m &= \gamma_2\,(1-\tau)\,\tau\,\epsilon_N\,P_o \end{aligned} \tag{75}$$

Substitution of (75) into (74) gives:

$$P_s = 2\gamma_1\gamma_2\,\tau(1-\tau)\,P_o\sqrt{\epsilon_N} \tag{76}$$

The value of τ which maximizes P_s is:

$$\tau = \frac{1}{2} \tag{77}$$

Thus:

$$P_s = \frac{1}{2} \gamma_1 \gamma_2 P_o \sqrt{\epsilon_N} \tag{78}$$

If, for example, we take

$$P_o = 10^{-3} \text{ watt}$$
$$\gamma_1 = 10^{-3}$$
$$\gamma_2 = .2$$
$$\epsilon_N = .01\%$$

then,

$$P_s = 10^{-9} \text{ watt} \tag{79}$$

Since the signal is at a fixed frequency and a narrow noise bandwidth (of the order of 1 Hz) is desirable, syncronous detection can be used to advantage. Silicon detectors should, therefore, suffice for phase measurements to $\pm .1$ radian (i.e., $\pm \lambda_o/125$ in terms of mirror deformation).

If, however, a diffraction efficiency, ϵ_N, much below .01% is used, it will be necessary to use more elaborate electronics or a stronger laser.

2.4 Appendices

2.4.1 Diffraction Analysis

2.4.1.1 Type "A" Zones

We are interested in the relative amount of light diffracted into orders N = 0 and N = 1. The angular dependence is practically identical for orders N = 0 and N = 1. Therefore, for all practical purposes we may simply compare the peak intensities.

We let:

I_o' = Peak intensity for order N = 0, assuming the zones to be absent.

I_o = Peak intensity for order N = 0 (when the zones are present).

I_1 = Peak intensity for order N = 1.

We also define the following:

λ = Wavelength of starlight.

λ_o = Wavelength of the monitoring light.

N = Order of diffraction.

τ = Step height.

DIFFRACTION FROM TYPE "A" ZONES

N'=0

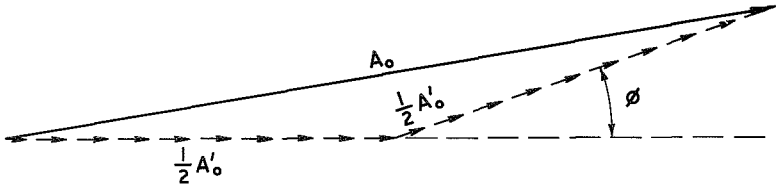

$$\phi = \frac{4\pi t}{\lambda}$$

$$A_o = A'_o \cos\frac{\phi}{2}$$

$$\epsilon_\lambda = 1 - \left(\frac{A_o}{A'_o}\right)^2 = \sin^2\frac{\phi}{2}$$

(a)

N'=1

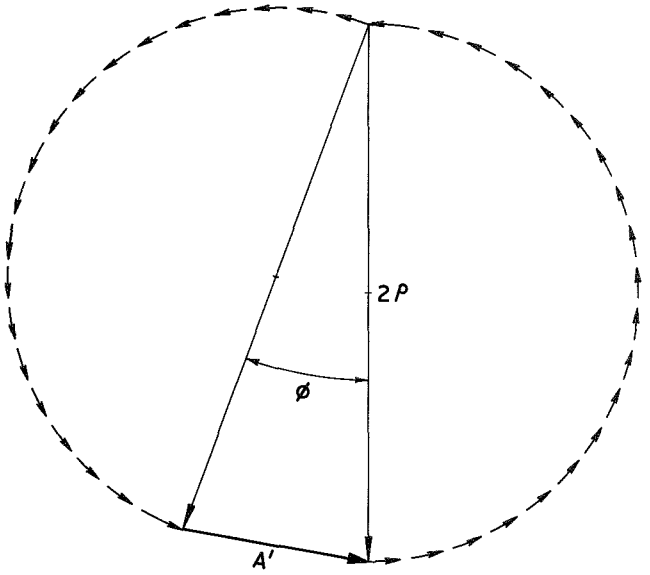

$$\phi = \frac{4\pi t}{\lambda}$$

$$A'_o = 2\pi P$$

$$A_1 = 4\pi \sin\frac{\phi}{2}$$

$$\epsilon_1 = \left(\frac{A_1}{A'_o}\right)^2 = \left[\frac{2}{\pi}\sin\frac{\phi}{2}\right]^2$$

(b)

FIGURE 9

ϵ_λ = Diffraction efficiency for all orders combined (except N = 0), at wavelength λ .

ϵ_1 = Diffraction efficiency for order N = 1 at wavelength λ_0 .

We also define the following field amplitudes:

$$A_c' = \sqrt{I_o'}$$
$$A_o = \sqrt{I_o} \qquad (80)$$
$$A_1 = \sqrt{I_1}$$

Hence:

$$\epsilon_\lambda = \frac{I_o'(\lambda) - I_o(\lambda)}{I_o'(\lambda)} = 1 - \left[\frac{A_o(\lambda)}{A_o'(\lambda)}\right]^2 \qquad (81)$$

$$\epsilon_1 = \frac{I_1(\lambda_o)}{I_1'(\lambda_o)} = \left[\frac{A_1(\lambda_o)}{A_1'(\lambda_o)}\right]^2 \qquad (82)$$

Neglecting very small obliquity effects, the integration of any component of the field amplitude over one complete zone period may be represented graphically in the complex plane as shown in Figure 9a (for N = 0) and in Figure 9b (for N = 1). The net contributions from successive zones are all in phase. Integration over a single zone suffices to give the proper ratios for N = 0 and N = 1.

As far as ratios are concerned, the integrated curve length (short arrows) may be considered as representing A_o'. The resultant vector then represents A_c in Figure 9a and A_1 in Figure 9b .

For order N = 0, the phase is constant over each half-zone. There is a phase jump of $\phi = \frac{4\pi\tau}{\lambda}$ due to the step height, τ, between the half-zones. From figure 9a it follows that:

$$A_0 = A_0' \cos\frac{\phi}{2} \tag{83}$$

Substitution of (83) into (81) gives:

$$\boxed{\epsilon_\lambda \approx \sin^2\frac{\phi}{2}} \tag{84}$$

Where:

$$\boxed{\phi = \frac{4\pi t}{\lambda}} \tag{85}$$

For order N = 1, the phase varies uniformly through half a cycle over each half-zone. There is again a phase jump of ϕ due to the step height, τ, between the two half-zones. From Figure 9b it follows that:

$$\begin{aligned} A_0' &= 2\pi\rho \\ A_1 &= 4\pi \sin\frac{\phi}{2} \end{aligned} \tag{86}$$

Substitution of (86) into (82) gives:

$$\boxed{\epsilon_1 = \left[\frac{2}{\pi}\sin\frac{\phi}{2}\right]^2} \tag{87}$$

where,

$$\boxed{\phi = \frac{4\pi t}{\lambda_0}} \tag{88}$$

Since $\phi << \frac{\pi}{2}$, the following approximation for (87) is valid:

$$\epsilon_1 \approx \left(\frac{4t}{\lambda_0}\right)^2 \tag{89}$$

DIFFRACTION FROM TYPE "B" ZONES

$N'=0$

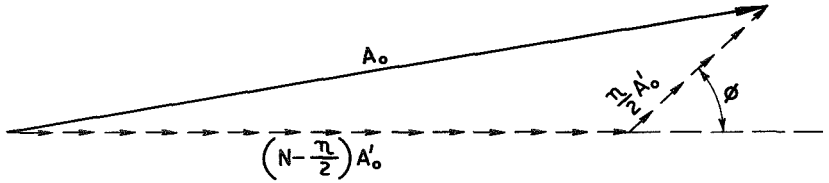

$$\phi=\frac{4\pi t}{\lambda}=\frac{\pi\lambda_o}{\lambda}$$

$$A_o^2=\left[\left(N-\frac{\eta}{2}\right)A'_o\right]^2+\left[\frac{\eta}{2}A'_o\right]^2+\left(N-\frac{\eta}{2}\right)\eta\left(A'_o\right)^2\cos\phi$$

$$\epsilon_\lambda=1-\left(\frac{A_o}{A'_o}\right)^2=2\left(1-\frac{\eta}{2N}\right)\frac{\eta}{N}\sin^2\phi$$

(a)

$N'\neq 0$

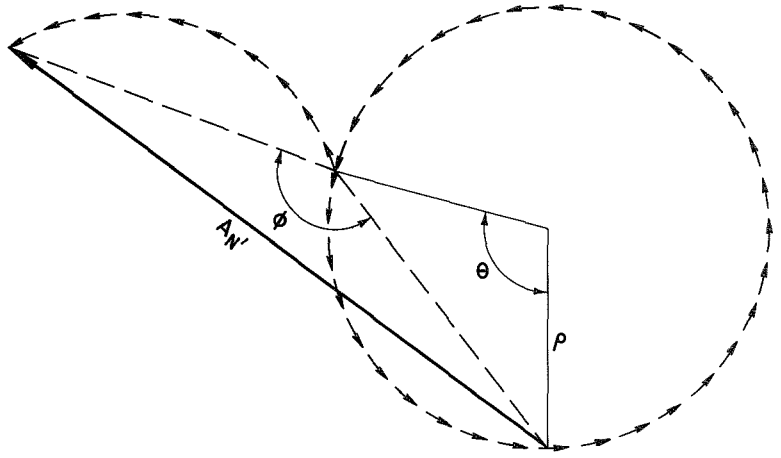

$$\theta=\pi\eta\frac{N'}{N}$$

$$\phi=\frac{4\pi t}{\lambda}=\frac{\pi\lambda_o}{\lambda}$$

$$A'_o=2\pi\rho N'$$

$$A_{N'}=4\rho\sin\frac{\theta}{2}\sin\frac{\phi}{2}$$

$$\epsilon_{N'}=\left(\frac{A_{N'}}{A'_o}\right)^2=\left[\frac{2}{\pi N'}\sin\frac{\theta}{2}\sin\frac{\phi}{2}\right]^2$$

(b)

FIGURE 10

2.4.1.2 Type "B" Zones

As for type "A" zones, we are interested only in ratios. Since $a >> N\lambda_o$ (where a = zone period), the angular dependence is practically identical for orders $N' \leq N$. We therefore use the same analysis as for type "A" zones.

In addition to the previous definitions, we define:

$I_{N'}$ = Peak intensity for order N'.

$\epsilon_{N'}$ = Diffraction efficiency for order N' at wavelength λ .

$A_{N'} = \sqrt{I_{N'}}$

$2Nb$ = Full zone period.

ηb = Width of the narrower region only.

As in the case of type "A" zones, we have:

$$\epsilon_\lambda \approx \frac{I_o'(\lambda) - I_o(\lambda)}{I_o'(\lambda)} = 1 - \left[\frac{A_o(\lambda)}{A_o'(\lambda)}\right]^2 \qquad (90)$$

$$\epsilon_{N'} \approx \frac{I_{N'}(\lambda)}{I_o'(\lambda)} = \left[\frac{A_{N'}(\lambda)}{A_o'(\lambda)}\right]^2 \qquad (91)$$

The amplitude integrals are shown schematically in Figures 10a and 10b.

For order N = 0, the phase is constant over both the narrower and the wider regions. There is a phase jump $\phi = \frac{\pi\lambda_o}{\lambda}$ due to the step height, $\frac{\lambda_o}{\gamma}$, between the two regions.

From Figure 10a, it follows from the cosine law that:

$$A_o^2 = \left[\left(1-\frac{\eta}{2N}\right)A_o'\right]^2 + \left[\frac{\eta}{2N}A_o'\right]^2 - \left(1-\frac{\eta}{2N}\right)\frac{\eta}{N}(A_o')^2\cos\phi \qquad (92)$$

Substitution of (92) into (90) gives:

$$\boxed{\epsilon_\lambda \approx 2\left(1-\frac{\eta}{2N}\right)\frac{\eta}{N}\sin^2\frac{\phi}{2}} \qquad (93)$$

Where:

$$\boxed{\phi = \frac{4\pi t}{\lambda} = \frac{\pi\lambda_o}{\lambda}} \qquad (94)$$

For order N', the phase varies continuously through $\frac{\eta N'}{2N}$ cycles over the narrower region and it varies through $N-\frac{\eta N'}{2N}$ cycles over the wider region. There is a phase jump of $\phi=\frac{\pi\lambda_o}{\lambda}$ due to the step height, $\frac{\lambda_o}{4}$, between the two regions.

From figure 10b it follows that:

$$A_o' = 2N'\pi\rho$$
$$A_{N'} = 4\rho\sin\frac{\theta}{2}\sin\frac{\phi}{2} \qquad (95)$$

Substitution of (95) into (91) gives:

$$\boxed{\epsilon_{N'} \approx \left[\frac{2}{\pi N'}\sin\frac{\theta}{2}\sin\frac{\phi}{2}\right]^2} \qquad (96)$$

Where:

$$\boxed{\theta = \pi\eta\frac{N'}{N}} \qquad (97)$$

$$\boxed{\phi = \frac{4\pi t}{\lambda} = \frac{\pi\lambda_o}{\lambda}} \qquad (98)$$

For order $N'=N$, this reduces to:

$$\boxed{\epsilon_N \approx \left[\frac{2}{\pi N}\sin\left(\frac{\eta\pi}{2}\right)\right]^2} \qquad (99)$$

2.4.2 Aberation Analysis of a Holographically Generated Zone Pattern

The zone pattern should be such that a monitoring wave diverging from the focus will be diffracted back to the focus. Such a pattern may be generated holographically by interference of two coherent waves. Ideally (as shown in Figure 6) one wave should diverge from the focus and the other wave should be a plane wave approaching on axis. The wavelength, λ_o, is the same as that used for monitoring.

Practically, however, it is very difficult to produce a wave that is truly plane over a large aperture. It is fortunate, therefore, that the pattern changes very little if the compromise geometry shown in Figure 6 is used. The wavelength, λ, of the light used to generate the pattern must be reduced accordingly. In practice one must select an available laser wavelength and choose the distances α F and β F accordingly.

The following is an analysis of the aberations in the fringe pattern introduced by the compromise geometry. Any aspherising effect of a secondary mirror on the shape of the monitoring wave is not included.

ZONE GEOMETRY

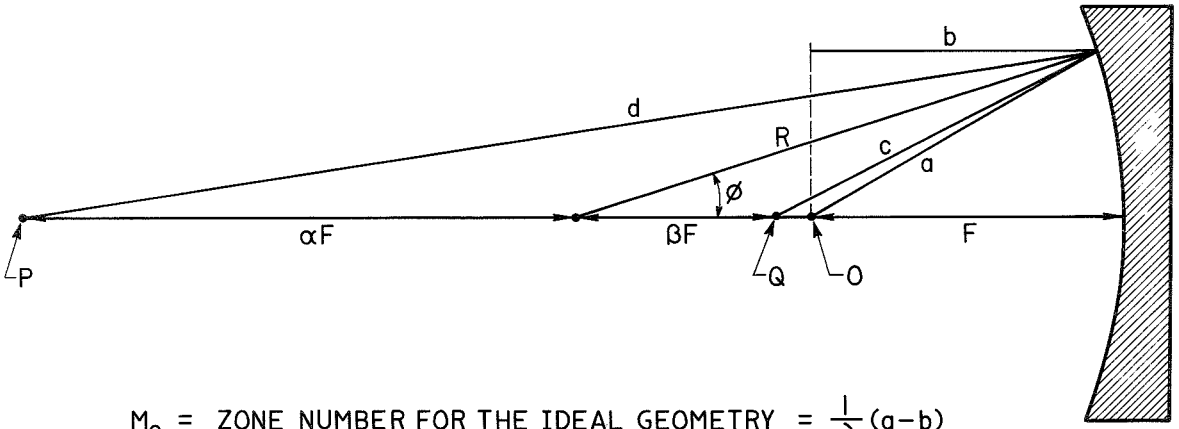

M_0 = ZONE NUMBER FOR THE IDEAL GEOMETRY = $\frac{1}{\lambda_0}(a-b)$

M_0 = ZONE NUMBER FOR THE COMPROMISE GEOMETRY = $\frac{1}{\lambda}(\alpha F + BF + c - d)$

2F = RADIUS OF THE BEST FITTING SPHERE

$a^2 = R^2 + F^2 - 2RF \cos \phi$

$b = R \cos \phi - F$

$c^2 = R^2 + (\beta F)^2 - 2R(\beta F) \cos \phi$

$d^2 = R^2 + (\alpha F)^2 + 2R(\alpha F) \cos \phi$

ZONE ABERRATION: $M_0 M = \frac{1}{\lambda_0}(a-b) - \frac{1}{\lambda}(\alpha F + BF + c - d)$

FIGURE 11

2.4.2.1 Calculation of the Focal Distances

The basic geometrical relationships are given in Figure 11. Parameters α & β are to be chosen so as to minimize the aberration ΔM. In the remainder of this section it will be shown that this results in the following formulae for α & β :

$$\alpha = \frac{4\gamma^2 - \gamma - 2 + \sqrt{4 - 3\gamma^2}}{2\gamma(1-\gamma)} \qquad \text{(a)}$$

$$\beta = \frac{4\gamma^2 + \gamma - 2 + \sqrt{4 - 3\gamma^2}}{2\gamma(1+\gamma)} \qquad \text{(b)} \qquad (100)$$

Where: $$\gamma = \frac{\lambda}{\lambda_0} \qquad \text{(c)}$$

For the ideal geometry, the interference pattern on the mirror consists of circular fringes formed by interference between a plane wave and a wave diverging from focal point O. The fringe number (counted from the center) is given by:

$$M_0 = \frac{1}{\lambda_0}(a - b) \qquad (101)$$

For the compromise geometry, the interference pattern consists of circular fringes formed by interference between a wave diverging from point P and a second wave diverging from point Q. The fringe number (counted from the center) is given by:

$$M = \frac{1}{\lambda}(\alpha F + \beta F + c - d) \qquad (102)$$

The difference in fringe number represents the aberration arising from the compromise geometry:

$$\Delta M = \frac{1}{\lambda_0}(a-b) - \frac{1}{\lambda}(\alpha F + \beta F + c - d) \tag{103}$$

Application of the Cosine Law to Figure 11 gives the following relations:

$$\left.\begin{aligned} a^2 &= R^2 + F^2 - 2RF\cos\phi \\ b &= R\cos\phi - F \\ c^2 &= R^2 + (\beta F)^2 - 2R\beta F\cos\phi \\ d^2 &= R^2 + (\alpha F)^2 + 2R\alpha F\cos\phi \end{aligned}\right\} \tag{104}$$

We choose the best-fitting sphere of radius 2F and denote the interval between the mirror surface and this sphere by $2F\delta_0$:

$$2F\delta_0 = R - 2F \tag{105}$$

or:

$$R = 2F(1+\delta_0) \tag{106}$$

δ_0 is very small.

We also define:

$$\nu = 1 - \cos\phi \tag{107}$$

ν is also small but not as small as δ_0.

Combining (105) and (107) with (104) gives:

$$\left.\begin{aligned} a^2 &= F^2[1 + 4\nu + 4\delta_0(1+\nu+\delta_0)] \\ b &= F[1 - 2\nu + 2\delta_0(1-\nu)] \\ c^2 &= F^2[(2-\beta)^2 + 4\beta\nu + 4\delta_0(2-\beta+\beta\nu+\delta_0)] \\ d^2 &= F^2[(2+\alpha)^2 - 4\alpha\nu + 4\delta_0(2+\alpha-\alpha\nu+\delta_0)] \end{aligned}\right\} \tag{108}$$

We define:

$$\left.\begin{aligned} \Delta_a &= 4\delta(1+v+\delta_0) \\ \Delta_b &= 2\delta(1-v) \\ \Delta_c &= 4\delta(2-B+Bv+\delta_0) \\ \Delta_d &= 4\delta(2+\alpha-\alpha v+\delta_0) \end{aligned}\right\} \quad (109)$$

Using Definitions (109) in (108) gives:

$$\left.\begin{aligned} a &= F\left[1+4v+\Delta_a\right]^{\frac{1}{2}} \\ b &= F\left[1-2v+\Delta_b\right] \\ c &= F\left[(2-B)^2+4Bv+\Delta_c\right]^{\frac{1}{2}} \\ d &= F\left[(2+\alpha)^2-4\alpha v+\Delta_d\right]^{\frac{1}{2}} \end{aligned}\right\} \quad (110)$$

We use the Binomial theorem to expand (110) up to terms of 1st order in δ_0 and 3rd order in v :

$$\left.\begin{aligned} a &= F\left[1+2v-2v^2+4v^3+\frac{\Delta_a}{2}-v\Delta_a\right] \\ b &= F\left[1-2v+\Delta_b\right] \\ c &= F\left[(2-B)+\frac{2Bv}{(2-B)}-\frac{2B^2v^2}{(2-B)^3}+\frac{4B^3v^3}{(2-B)^5}-\frac{Bv\Delta_c}{(2-B)^3}+\frac{\Delta_c}{2(2-B)}\right] \\ d &= F\left[(2+\alpha)-\frac{2\alpha v}{(2+\alpha)}-\frac{2\alpha^2v^2}{(2+\alpha)^3}-\frac{4\alpha^3v^3}{(2+\alpha)^5}+\frac{\alpha v\Delta_d}{(2+\alpha)^3}+\frac{\Delta_d}{2(2+\alpha)}\right] \end{aligned}\right\} \quad (111)$$

Terms in δ_o and v^3 are very small. We therefore drop these and all higher terms from (111):

$$\left.\begin{aligned} a &= F\left[1 + 2v - 2v^2\right] \\ b &= F\left[1 - 2v\right] \\ c &= F\left[(2-B) + \frac{2Bv}{(2-B)} - \frac{2B^2v^2}{(2-B)^3}\right] \\ d &= F\left[(2+\alpha) - \frac{2\alpha v}{(2+\alpha)} - \frac{2\alpha^2v^2}{(2+\alpha)^3}\right] \end{aligned}\right\} \quad (112)$$

Substitution of (112) into (103) gives:

$$\frac{1}{\lambda_o}\left[4v - 2v^2\right] = \frac{1}{\lambda}\left[\frac{2Bv}{(2-B)} + \frac{2\alpha v}{(2+\alpha)} - \frac{2B^2v^2}{(2-B)^3} + \frac{2\alpha^2v^2}{(2+\alpha)^3}\right] \quad (113)$$

Equating terms in v gives:

$$\frac{2}{\lambda_o} = \frac{1}{\lambda}\left[\frac{B}{(2-B)} + \frac{\alpha}{(2-\alpha)}\right] \quad (114)$$

Equating terms in v^2 gives:

$$\frac{1}{\lambda_o} = \frac{1}{\lambda}\left[\frac{B^2}{(2-B)^3} - \frac{\alpha^2}{(2+\alpha)^3}\right] \quad (115)$$

We make the following substitutions:

$$2 - g = B \quad (116)$$

$$h - 2 = \alpha \quad (117)$$

(114) and (115) thus become:

$$\frac{2}{\lambda_o} = \frac{1}{\lambda}\left[\frac{(2-g)}{g} + \frac{(h-2)}{h}\right] \quad (118)$$

$$\frac{1}{\lambda_o} = \frac{1}{\lambda}\left[\frac{(2-g)^2}{g^3} - \frac{(h-2)^2}{h^3}\right] \quad (119)$$

Cross multiplication of (118) with (119) gives:

$$2(2-g)^2h^3-2(h-2)^2g^3=g^2h^3(2-g)+g^3h^2(h-2) \tag{120}$$

(120) reduces to:

$$(1-g)\,h^3=(1-h)\,g^3 \tag{121}$$

Solving (118) for g and h gives:

$$g=\frac{h}{1+\gamma h} \tag{122}$$

$$h=\frac{g}{1-\gamma g} \tag{123}$$

where:

$$\gamma=\frac{\lambda}{\lambda_0} \tag{124}$$

Substitution of (123) into (121) gives:

$$(1-g)g^3=\left[(1-\gamma g)^3-(1-\gamma g)^2g\right]g^3 \tag{125}$$

$$(1-g)=1-3\gamma g+3\gamma^2g^2-\gamma^3g^3-g+2\gamma g^2-\gamma^2g^3 \tag{126}$$

(126) reduces to:

$$\gamma(1+\gamma)g^2-(2+3\gamma)g+3=0 \tag{127}$$

The solution of (127) is:

$$g=\frac{2+3\gamma-\sqrt{4-3\gamma^2}}{2\gamma(1+\gamma)} \tag{128}$$

The sign of the radical in (128) is determined by the fact that

$$g = 1 \quad \text{when} \quad \gamma = 1.$$

Relations (122), (123) and (124) are invariant under the following transformation:

$$g \longrightarrow h$$
$$h \longrightarrow g$$
$$\gamma \longrightarrow -\gamma$$

Applying this transformation to (128) gives:

$$h = \frac{-(2-3\gamma) + \sqrt{4-3\gamma^2}}{2\gamma(1-\gamma)} \tag{129}$$

Substitution of (116) into (128) and substitution of (117) into (129) proves (100).

2.4.2.2 Calculation of the Aberrations

The parameters α & β have been chosen so that (111) is identically satisfied (103) up to terms of 2nd order in v. These terms therefore do not contribute to ΔM. Substitution of the remaining terms into (103) gives:

$$\Delta M = \frac{F}{\lambda_0}\left[4v^3 + \frac{\Delta_a}{2} - v\Delta_a - \Delta_b + \cdots\right]$$
$$- \frac{F}{\lambda}\left[\frac{4\beta^3 v^3}{(2-\beta)^5} + \frac{4\alpha^3 v^3}{(2+\alpha)^5} - \frac{\beta v \Delta_c}{(2-\beta)^3} - \frac{\alpha v \Delta_d}{(2+\alpha)^3}\right. \quad (130)$$
$$\left. + \frac{\Delta_c}{2(2-\beta)} - \frac{\Delta_d}{2(2+\alpha)} + \cdots\right]$$

We substitute (109) into (130) and ignore all terms above 3rd order in v and above 1st order in δ :

$$\Delta M = \frac{4F}{\lambda_0} v^3 - \frac{4F}{\lambda}\left[\frac{\beta^3}{(2-\beta)^5} + \frac{\alpha^3}{(2+\alpha)^5}\right]$$
$$- \frac{2F}{\lambda}\left[\frac{\beta}{(2-\beta)} + \frac{\alpha}{(2+\alpha)} - \frac{2\beta}{(2-\beta)^2} - \frac{2\alpha}{(2+\alpha)^2}\right] \quad (131)$$

Use of (114) and (100c) simplifies (131) to:

$$\Delta M = \frac{4F}{\lambda_0}\left[U v^3 + W v \delta_0\right] \quad (132)$$

where:

$$\left.\begin{aligned} \gamma U &= \gamma - \frac{\beta^3}{(2-\beta)^5} - \frac{\alpha^3}{(2+\alpha)^5} \\ \gamma W &= \frac{\beta}{(2-\beta)^2} + \frac{\alpha}{(2+\alpha)^2} - \gamma \end{aligned}\right\} \quad (133)$$

(133) and (134) may be reexpressed in terms of γ. For this purpose the following relations are useful:

$$\frac{1}{g} = \frac{1}{6}\left[2 + 3\gamma + \sqrt{4-3\gamma^2}\right] \tag{134}$$

$$\frac{1}{h} = \frac{1}{6}\left[2 - 3\gamma + \sqrt{4-3\gamma^2}\right] \tag{135}$$

Relations (134) and (135) are derived from (127) in the same way as (128) and (129).

Using (116) and (117), we reexpress (133) and (134) in terms of g and h:

$$\gamma U = \gamma - \frac{(2-g)^3}{g^5} - \frac{(h-2)^3}{h^5} \tag{136}$$

$$\gamma W = \frac{(2-g)}{g^2} + \frac{(h-2)}{h^2} - \gamma \tag{137}$$

Expansion of (136) and (137) gives:

$$\gamma U = \gamma - 8\left(\frac{1}{g^5} - \frac{1}{h^5}\right) + 12\left(\frac{1}{g^4} - \frac{1}{h^4}\right) - 6\left(\frac{1}{g^3} - \frac{1}{h^3}\right) + \left(\frac{1}{g} - \frac{1}{h}\right) \tag{138}$$

$$\gamma W = 2\left(\frac{1}{g^2} - \frac{1}{h^2}\right) - \left(\frac{1}{g} - \frac{1}{h}\right) \tag{139}$$

Substitution of (134) and (135) into (138) and (139) gives:

$$\left.\begin{aligned} U &= \frac{1}{81}\left[(67 - 120\gamma^2 + 72\gamma^4) - (7 + 12\gamma^2)\sqrt{4-3\gamma^2}\right] \\ W &= \frac{2}{3}\left[-1 + \sqrt{4-3\gamma^2}\right] \end{aligned}\right\} \tag{140}$$

We define:

$$\rho = 1 - \gamma \tag{141}$$

(140) and (141) may be represented by power series in ρ :

$$\left.\begin{aligned} U &= -\rho\left[1 - 6\rho + 10\rho^2 - 24\rho^3 + \cdots\right] \\ W &= 2\rho\left[1 - 2\rho + 6\rho^2 - 24\rho^3 + \cdots\right] \end{aligned}\right\} \tag{142}$$

Where: $\rho = \frac{\lambda}{\lambda_0}$

We also define:

$$(\Delta M') = \frac{4F\delta_0}{\lambda_0} \tag{143}$$

$(\Delta M')$ represents the difference (in fringes) between the surface of the mirror and the best-fitting sphere.

Using (107), we approximate v by:

$$v \approx \frac{\phi^2}{2} \tag{144}$$

Substitution of (143) and (144) into (132) gives:

$$(\Delta M) = -\left[\frac{F\phi}{2\lambda_0}\right] U(\gamma) + \left[\frac{\phi^2}{2}\right] W(\gamma)(\Delta M') \tag{145}$$

Where $U(\gamma)$ and $W(\gamma)$ are given by (134) or (140) or (142) or by the following table:

γ	$U(\gamma)$	$W(\gamma)$
1.0	0	0
.9	-.049	.167
.8	-.019	.293
.7	+.062	.393
.6	+.170	.473
.5	+.290	.533

The first term in (145) is due to the compromise geometry alone regardless of the asphericity of the mirror. As $\gamma \to 1$ (i.e., as the compromise geometry approaches the ideal geometry) $U(\gamma)$ goes to zero and the first aberration term vanishes. By a rather remarkable coincidence, $U(\gamma)$ has another zero at almost the exact value of γ (namely $\gamma = .771$) that results when an Argon laser ($@\lambda = 488\,nm$) is used to generate the zone pattern and a He-Ne laser ($@\lambda = 633\,nm$) is used to monitor the figure of the mirror.

The second term in (145) is due both to the compromise geometry and to the asphericity of the surface. As $\gamma \to 1$ (i.e., as the compromise geometry approaches the ideal geometry) $W(\gamma)$ goes to zero and the second aberration term vanishes. As $(\Delta M') \to 0$ (i.e., as the surface approaches the best-fitting sphere), the second term also vanishes.

As an example of the magnitude of the aberrations, we assume a parabolic mirror.

For a parabola:

$$(\Delta M')_{max} \approx \frac{F(\phi_{max})^4}{8 d_o} \tag{146}$$

We approximate (ϕ_{max}) by:

$$\phi_{max} \approx \frac{1}{4f} \tag{147}$$

Substitution of (146) and (147) into (145) gives:

$$(\Delta M')_{max} \approx -\left[\frac{D}{2^{13}\lambda_0 f^5}\right] U(\gamma) + \left[\frac{D}{2^{16}\lambda_0 f^5}\right] W(\gamma) \quad (148)$$

If, for example, we choose:

D = 3m

f = 4

λ_0 = 633 nm

γ = .7

Then:

$$(\Delta M')_{max} \approx .57\, U(\gamma) + .08\, W(\gamma)$$

$$\approx .09 \text{ fringes}$$

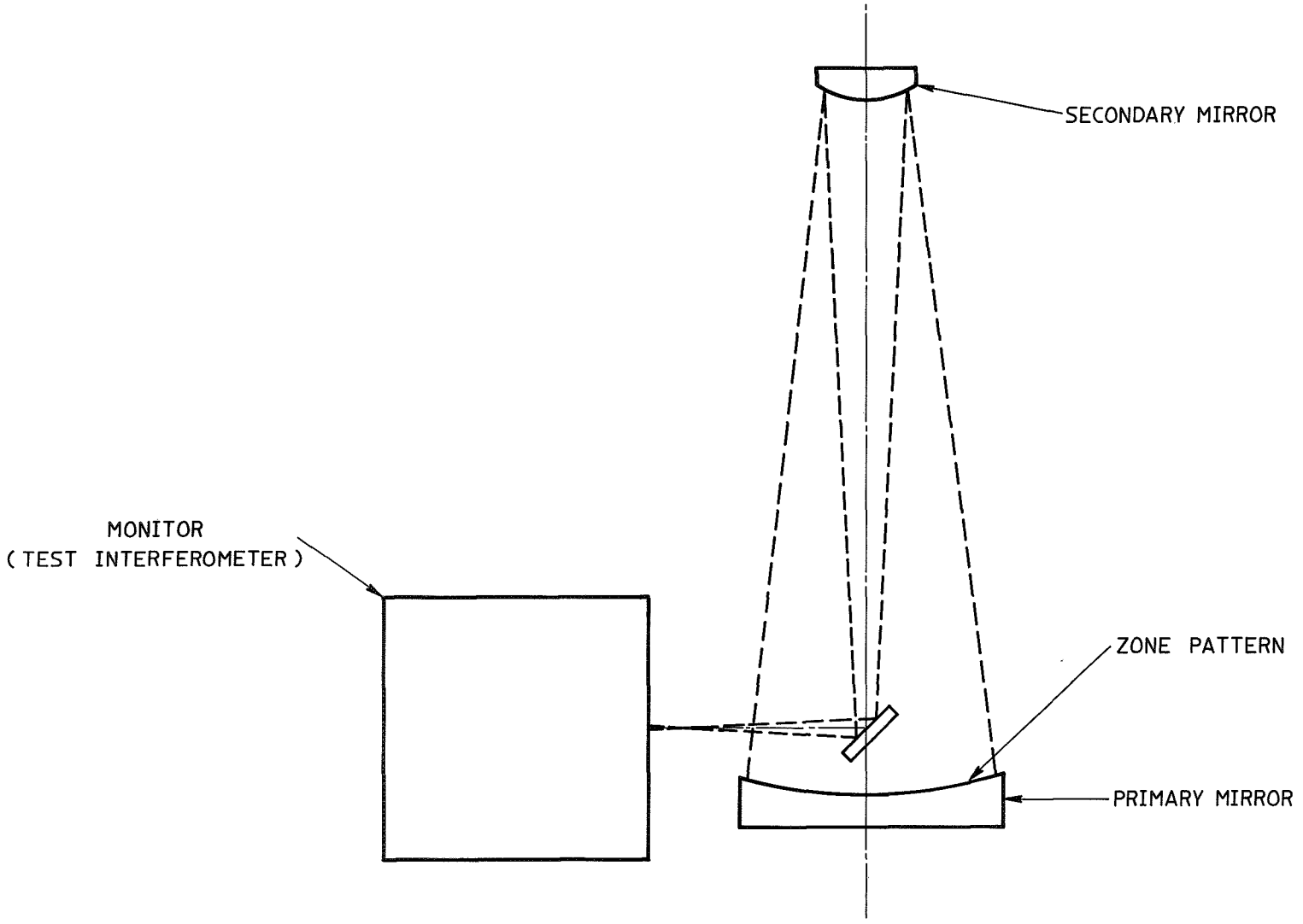

TELESCOPE AND MONITOR

FIGURE 12

EXPERIMENTAL STUDY

3.1 Telescope/Interferometer System

3.1.1 Telescope

The telescope (See Figures 12 , and 13) was of cassegranian structure. The major characteristics of the primary mirror were:

Diameter: 12 inches

Aperture Ratio: f/5

Material: Cer-Vit(R)

Both the primary and secondary mirrors were spherical to within $\pm \frac{\lambda}{10}$. The combination was used at an EFL of approximately 20 feet. A plane mirror was used to deflect the beam so that no hole was needed in the primary mirror. This plane mirror served also as an attenuator (see Section 3.3.2).

(R) Registered trademark of Owens-Illinois, Inc.

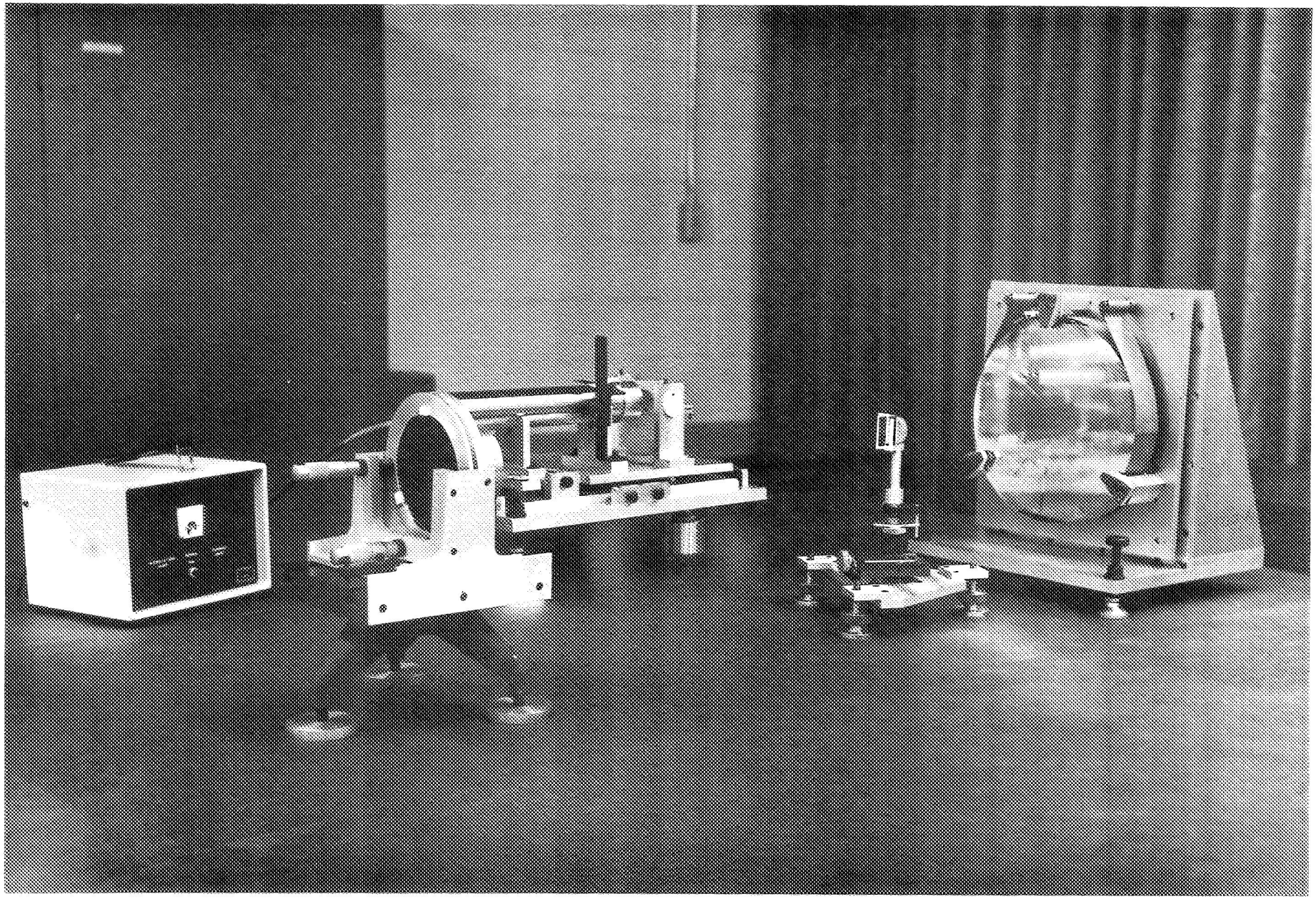

TELESCOPE AND MONITOR

FIGURE 13

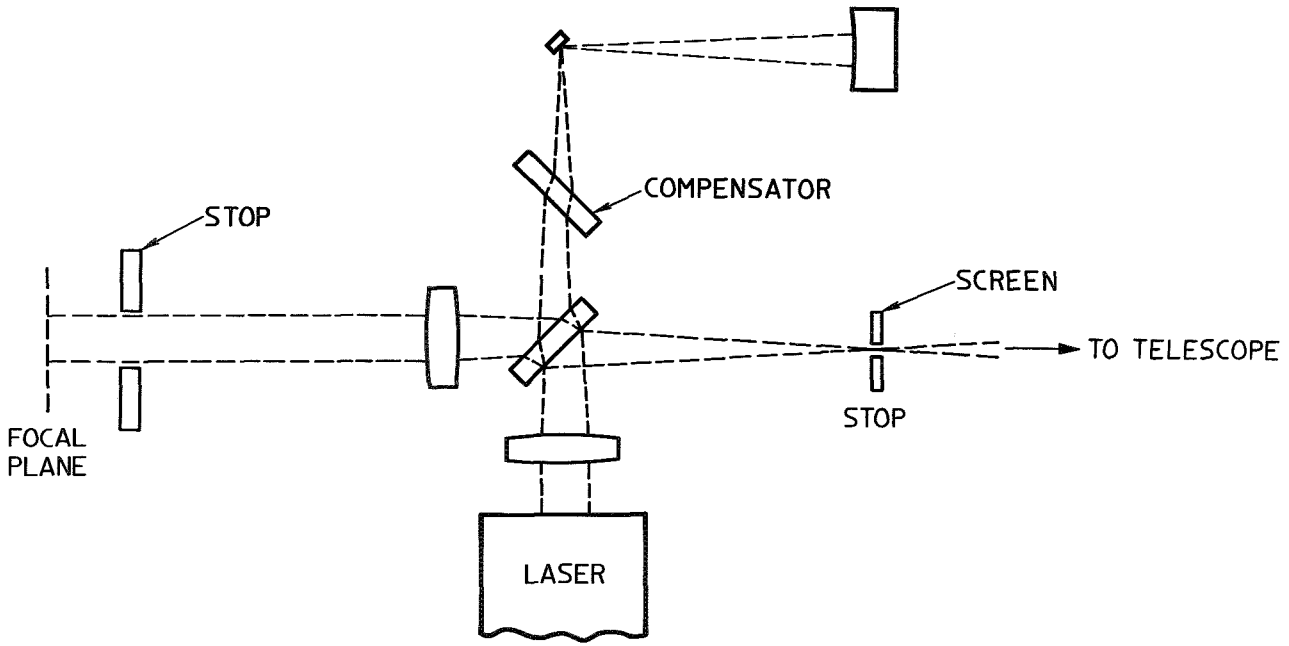

INTERFEROMETER

FIGURE 14

3.1.2 Interferometer

Figures 14 and 15 show the interferometer.

The source was a He-Ne laser with the following characteristics:

Wavelength: 633nm

Power: .5 milliwatts

Cavity length: 216mm

Mode structure: TEM_{oo}

Polarization: Linear

The gaussian exit beam was stopped down from a diameter (between the $\frac{1}{e^2}$ intensity points) of approximately 10mm to a diameter of 6mm. The power passing through this stop was .3 milliwatts.

Being unstabilized, the laser sometimes resonated at two frequencies. This, however, was of no consequence since the path difference in the interferometer was set at approximately a multiple of the cavity length.

In the design of the interferometer, care was taken to suppress stray reflections. No lenses were used in either the measuring beam or the reference beam. In consequence, light incident on the beamsplitter was not collimated. The decollimation, however, was so slight that the resulting astigmatism could be readily corrected with a compensating plate.

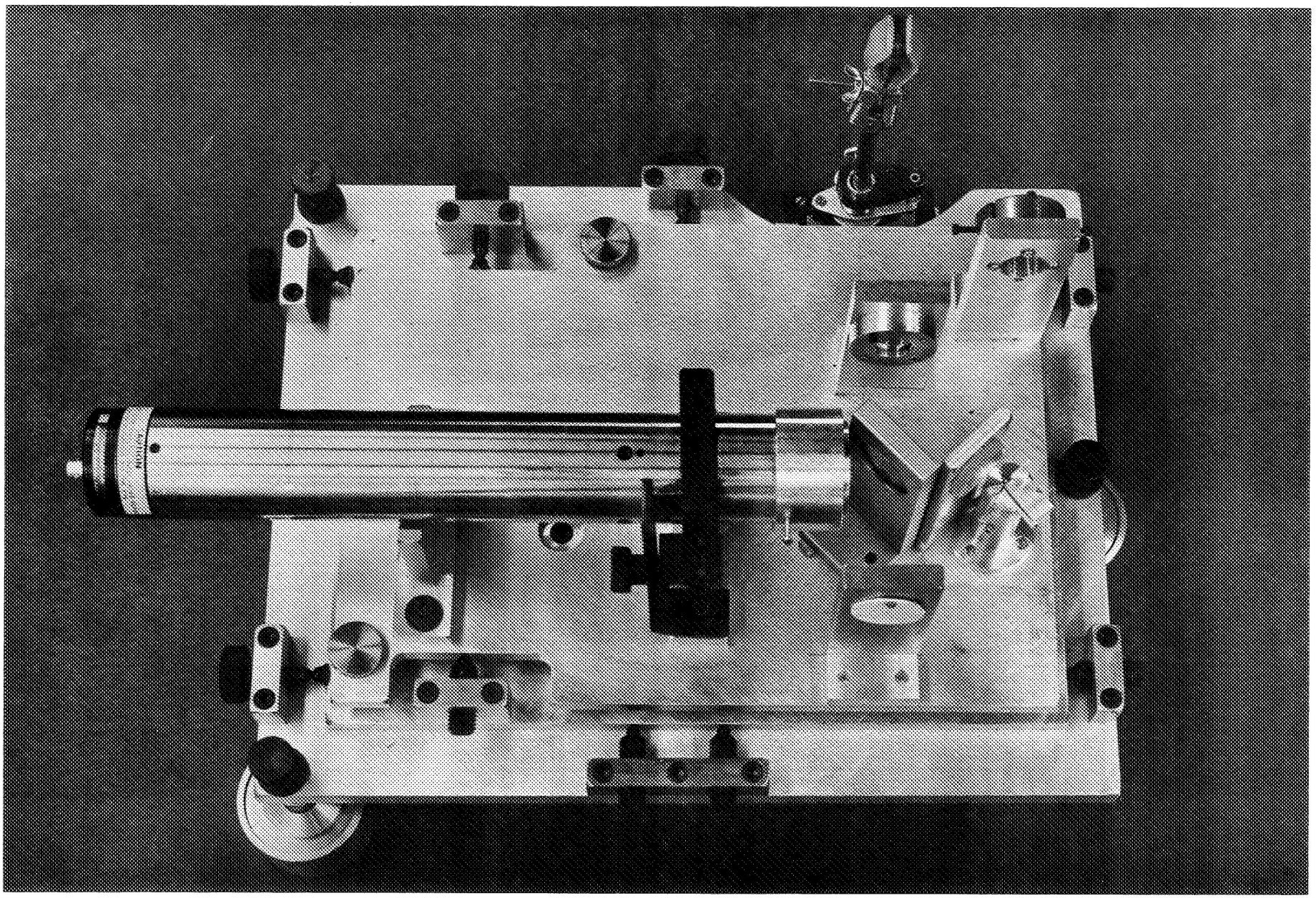

INTERFEROMETER

FIGURE 15

The small mirror near the focus of the reference beam served as an attenuator to match the intensity of the reference beam to that of the measuring beam. This was necessary only for photographic purposes; in a heterodyne sensing system (such as that in Figure 1) the reference beam would not be attenuated.

3.2 Generation of the Zone Pattern

It was originally proposed that the most suitable method of generating a large zone pattern would be to scribe it with a laser "stylus" under interferometric control. Funding limitations dictated, however, that a photographically generated zone pattern must suffice for this feasibility study. Calibration of the pattern was, therefore, not included in the experimental part of this study; not only would it have been costly, but its relevance to a pattern scribed under interferometric control is questionable. Care was taken, however, to keep the wavefront aberrations below about 1 μm.

3.2.1 Holographic Arrangement

3.2.1.1 Seismic Support and Shielding

As shown in Figures 16 and 17 the entire arrangement rested on a seismic block 30 feet in length. Pneumatic supports for this block reduce acceleration due to seismic disturbances by 12db/octave. for all frequencies above 3 Hz.

A section of the wooden tunnel used to protect the optical path against air currents also appears in Figures 16 and 17.

3.2.1.2 Laser Source

The source was a continuous wave argon laser with the following output characteristics:

Wavelength:	488 nm
Power:	300 milliwats
Beam Diameter:	~ 1.5 mm
Mode Structure:	TEM_{oo}
Polarization:	Linear

HOLOGRAPHIC ARRANGEMENT (LOOKING TOWARD THE MIRROR)

FIGURE 16

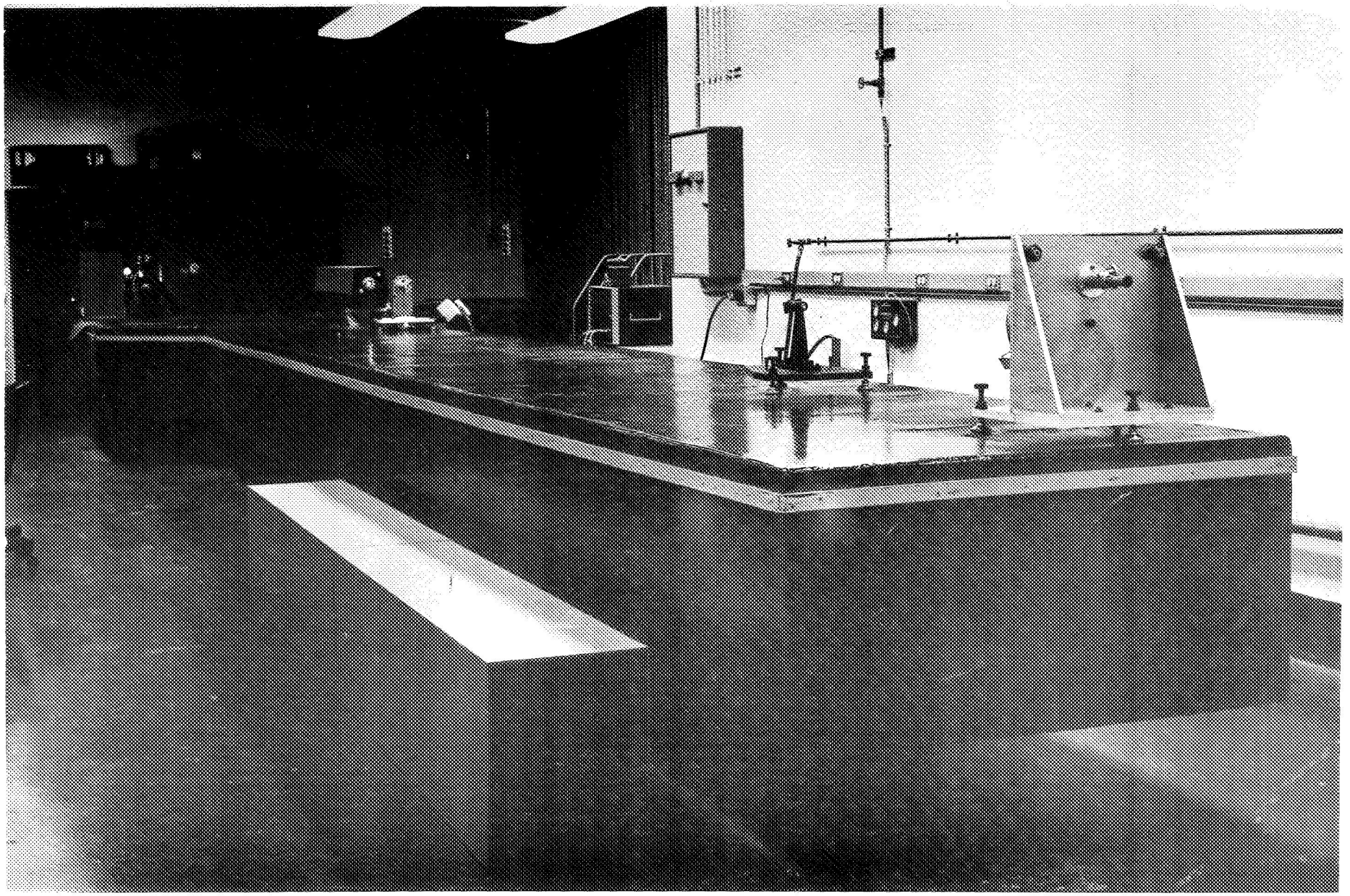

HOLOGRAPHIC ARRANGEMENT (LOOKING TOWARD THE LASER)

FIGURE 17

HOLOGRAPHIC ZONE PATTERN GENERATOR

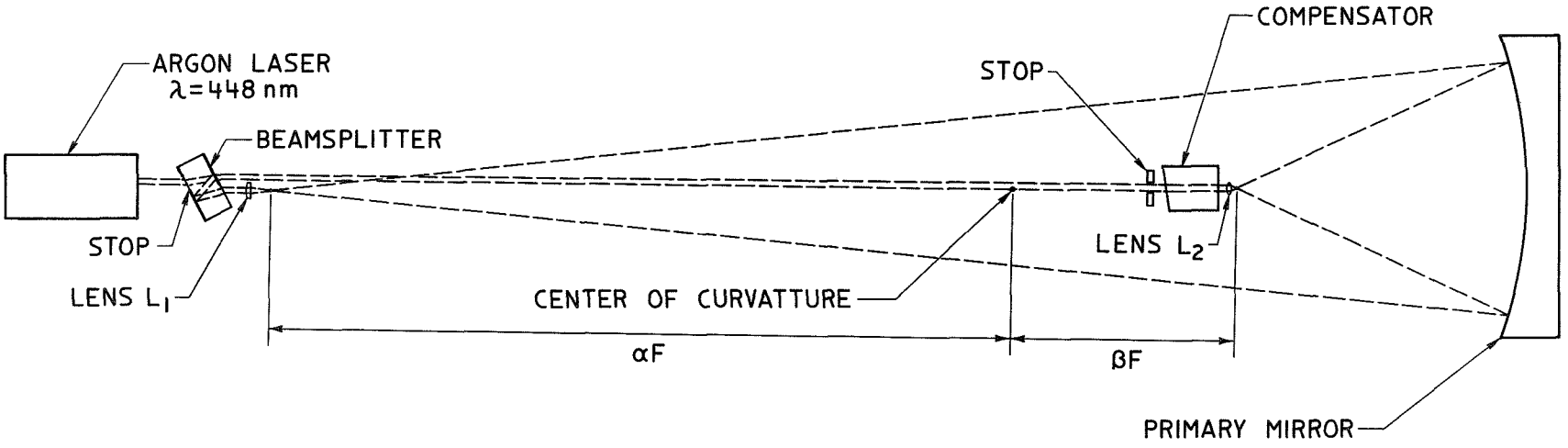

FIGURE 18

3.2.1.3 Optical Arrangement

The optical arrangement is shown in Figure 18. This arrangement used the compromise geometry shown in Figure 6 and analysed in Section 2.4.2. The parameters in this instance were:

$$\lambda = .488 \text{ nm}$$

$$\lambda_o = .632 \text{ nm}$$

$$F = 60.0 \text{ inches}$$

This resulted in the following values:

$$\alpha = 3.10$$

$$\beta = .966$$

$$\alpha F = 15'6''$$

$$\beta F = 57.6''$$

The beamsplitter assembly is shown in Figure 19. Very good optical quality and cleanliness were required in this assembly to reduce speckling due to scatter from the collimated beam.

For the sake of uniformity, the two interfering beams were diverged to cover an area considerably larger than the mirror. Because of the limited coherence of the argon laser, a compensator was required to equalize the mean path length of the two beams.

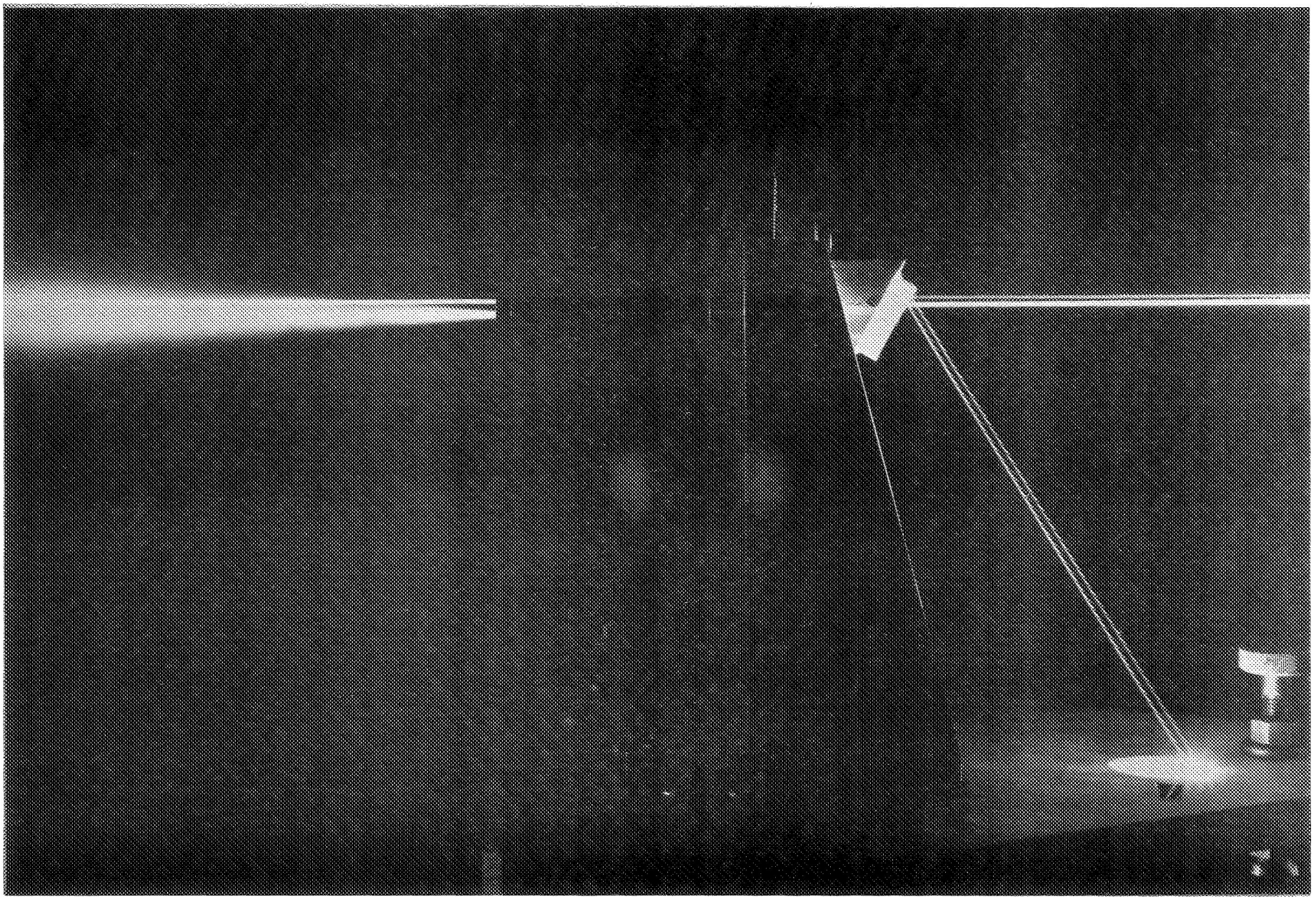

BEAMSPLITTER

FIGURE 19

3.2.2 Photosensitive Material

A relief pattern was desired in a durable substrate which could be cleaned and recoated without degrading the pattern. For this a photographic material was needed which would produce a wash-off pattern of bare zones through which the substrate could be etched or overcoated. The material had to have a sensitivity to laser light at λ = 488nm compatible with reasonable source intensity and exposure time. Resolution exceeding 130 line pairs/mm was also required.

The material finally chosen was Kodak Ortho Resist (KOR). Some experimentation was done with dichromated gelatin and with silver halide (etch-bleach process), but neither material showed any promise of being as satisfactory as (KOR). The sensitivity, resolution and adhesion of KOR proved entirely adequate. The relative ease with which it could be handled and coated onto large areas made it an obvious choice over silver halide and dichromated gelatin.

The most serious drawback of KOR (and photopolymers in general) for photography of fringe patterns is the high contrast required for good resolution of the images. In conjunction with the sinusoidal character of the fringes, this makes proper exposure difficult. The presence of stray light or movement of the fringes during exposure lowers the contrast and increases the difficulty.

3.2.3 Dipcoater

The dipcoater is shown in Figure 20. As the mirror blank was withdrawn from the tank, a compensating blank was lowered to keep the liquid level constant. The tank was made of stainless steel (recommended for KOR) and was wide enough to allow 1 inch clearance between the blanks.

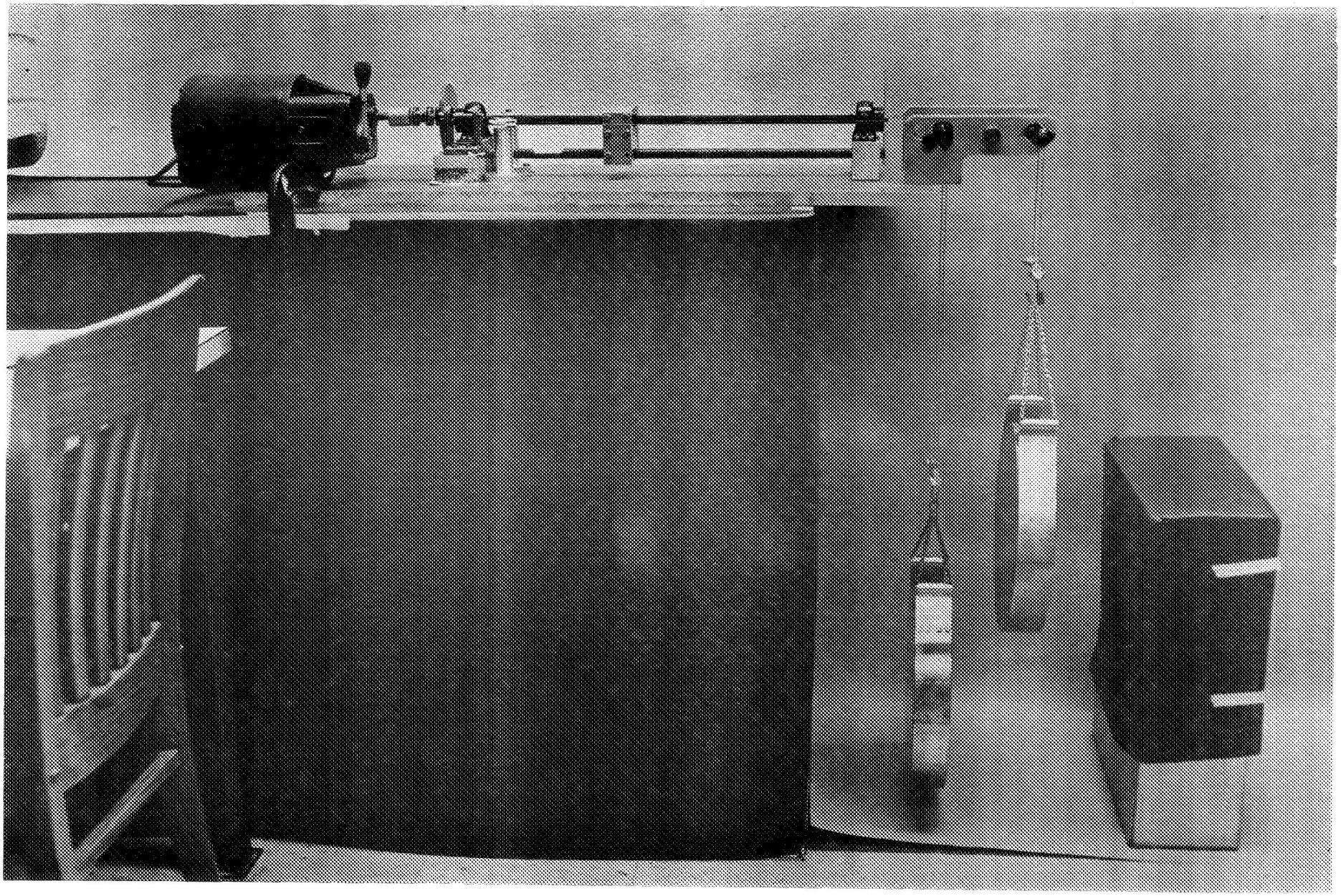

DIPCOATER

FIGURE 20

3.2.4 Photographic Procedure

The photographic procedure is one that can be used for fabricating zone plates (either reflective or transmissive) for purposes other than those associated with this particular study. We therefore present a fairly detailed description in the following sections.

3.2.4.1 Substrate Preparation

For use with KOR, a copper or chrome substrate is recommended. In the zone pattern used in this study, the substrate consisted of a copper layer 140nm thick evaporated onto a thin bonding layer of chrome.

After deposition of the metal substrate, it is desirable to coat the surface with photoresist while it is still uncontaminated. If, however, the substrate is reused or otherwise requires cleaning, the following procedure is recommended:

(a) Using surgical cotton, wash the surface with aerosol dissolved in warm water.

(b) Rinse with hot distilled water.

(c) Rinse dry with acetone (electronic grade).

3.2.4.2 Dipcoating

A stainless steel tank is recommended for KOR.

The blank should remain immersed in the KOR long enough to reach good thermal equilibrium. In the case of a 2" thick blank that has just been cleaned in hot water, a period of at least two hours is recommended.

In the dipping process, the following conditions were found to give good results:

Dilution: 1 part KOR to 2 parts KOR Thinner

Temperature: 72° F (22° C)

Withdrawal rate: 6 cm/minute

The withdrawal should be steady. Displacement of the liquid by the blank should be compensated (see Section 3.2.3). During withdrawal, a slight rippling of the liquid in the tank from high frequency vibrations has no adverse effect on the coating. Low frequency perturbations should be avoided.

Drip marks across the face of the blank may be prevented by holding the blank in a circular strap which is set back about 4 millimeters from the face of the blank.

After withdrawal, allow the blank to dry for 5 minutes while still hanging.

Warning: Do not breathe vapors from KOR or KOR Thinner.

3.2.4.3 Prebaking

Bake for 10 minutes at 170° F (77° C).

3.2.4.4 Exposure

High contrast in the exposure is essential. The fringes therefore must be sharp and stable.

To produce sharp fringes, stray light must be rigorously suppressed. Equalization of the beam paths and of the beam intensities at the mirror is also important but less critical. For an argon laser (operating in a single spectral line) it is sufficient if the optical paths match within ± 1 cm. An intensity mismatch of 3:2 can be tolerated.

Stability of the fringes is critical. Motion exceeding .1 fringe should be avoided. Shielding against atmospheric and seismic disturbances is therefore essential. Thermal drift in the geometry must also be low enough that fringe shift during exposure does not exceed .1 fringe.

The latitude allowed for proper exposure is only about $\pm$ 10%. The optimum exposure for each new set of conditions can therefore be established satisfactorily only by means of test exposures. In the present study, exposure times were of the order of 2 minutes. This corresponds to an exposure of roughly 40 Joul/m^2.

3.2.4.5 Development

(a) Soak the image in KOR Developer (@ 72° F) for 5 minutes. Agitate gently.

(b) Spray develop immediately with KOR Developer. Considerable hydraulic action is needed. It is desirable to use a sprayer which can apply a forceful spray to a large area so as to facilitate uniform development.

(c) Spray rinse with xylene.

Warning: Do not breathe vapors from KOR Developer.

3.2.4.6 Postbaking

Bake at 250° F (170° C) for 10 minutes.

3.2.4.7 Etching

The copper substrate used in this study was etched by immersion in a saturated solution of ferric chloride and water at 72° F (20° C).

Overetching should be avoided. The blank may be removed, washed and inspected during the etching process. A weaker solution for slower etching may be used if desired.

To remove the photoresist after etching:

(a) Immerse the surface in KOR Developer for 10 minutes. (Do not breathe the vapors.)

(b) Rub the surface gently with surgical cotton soaked in a solution of aerosol and warm water.

To clean the surface, use the procedure given in Section 3.2.4.1.

Instead of etching the surface to produce a relief image, a layer of copper or other material may be evaporated onto the regions that are bare of photoresist. Tests with copper showed good adhesion when the surface had been prepared as specified in Section 3.2.4.5.

3.2.5 Results

There are so many variables which affect the outcome that it was most gratifying to finally obtain a pattern of unexpectedly good quality.

3.2.5.1 Resolution

The resolution required varies inversely with the diameter up to a maximum of 158 line pairs/mm at a diameter of 12 inches. That the required resolution was achieved over most of the area can be seen from Figures 23 through 30.

In Figures 23 through 30 the outermost inch has been stopped out so that a diameter of 10 inches remains. In the outermost half-inch the coating was not usable due to surface tension effects in the dipcoating process. In the next half-inch the results were not uniform. Along the right edge of the field in Figures 23 through 30, a region can be seen where the zones failed to etch because they were not completely resolved during development of the photoresist.

Figure 21 shows the fringes at a diameter of 7" where the resolution is 92 line pairs/mm and Figure 22 shows the fringes at a diameter of 10" where the resolution is 132 line pairs/mm.

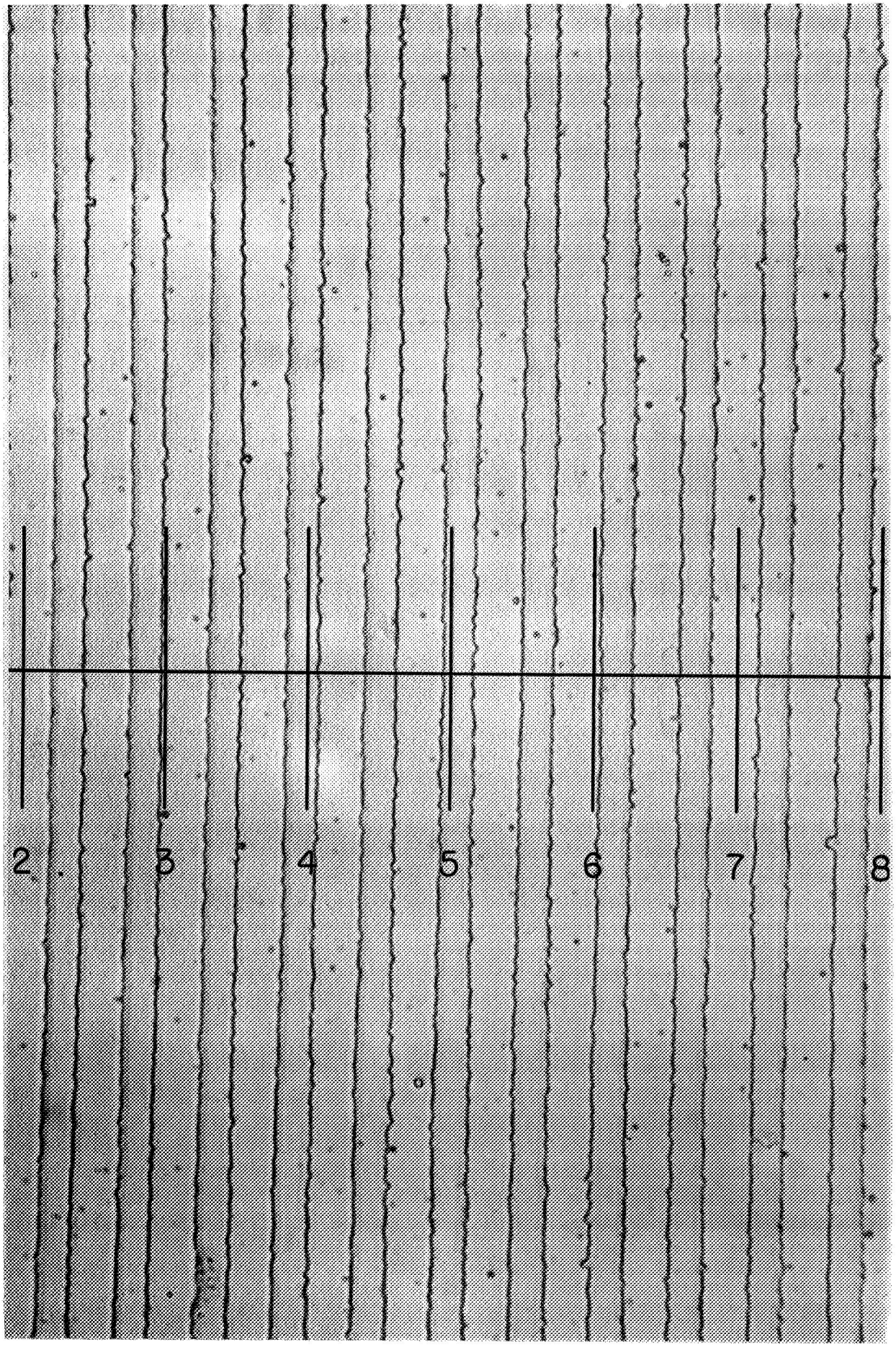

ZONE PATTERN (7" DIAMETER)

FIGURE 21

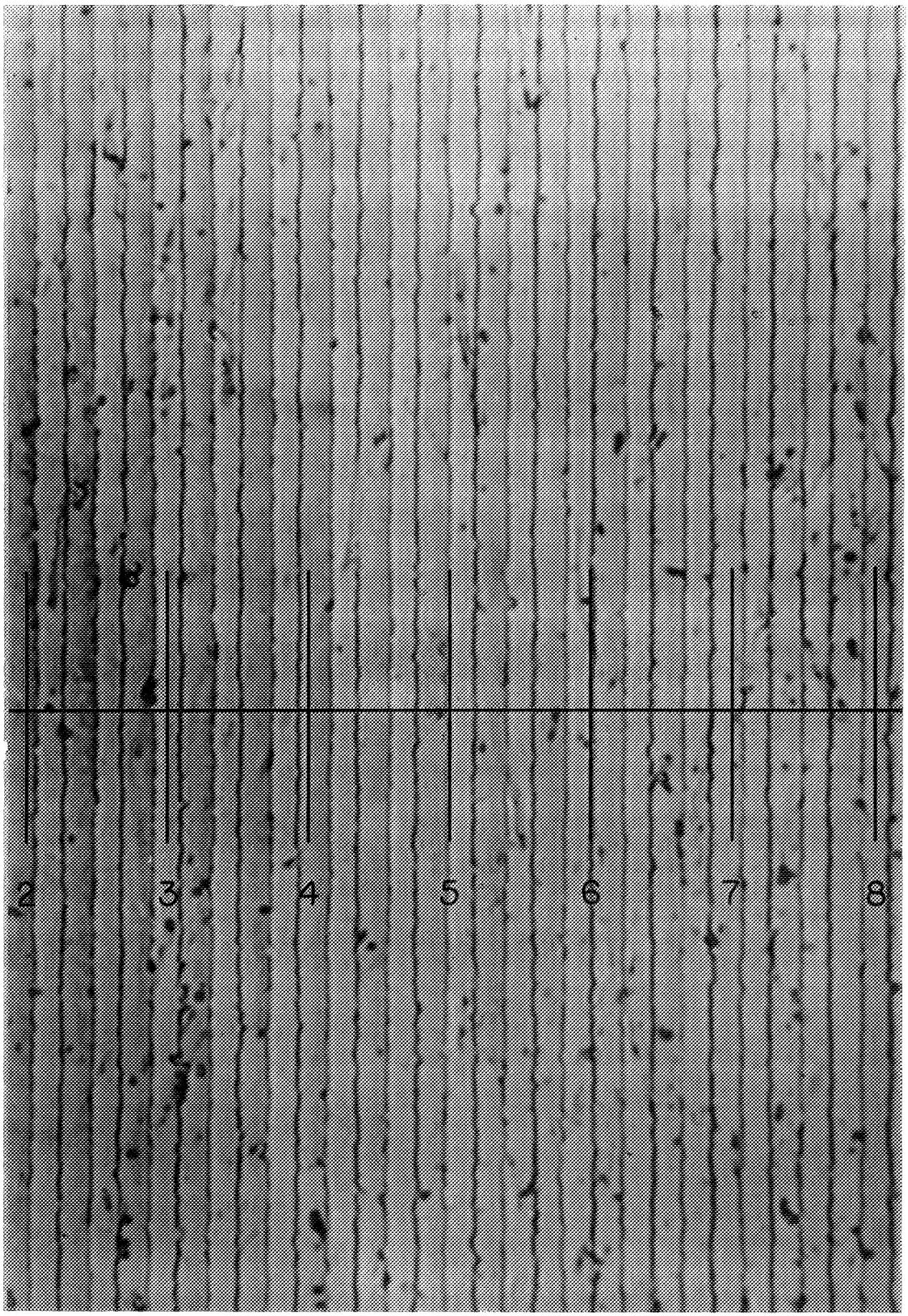

ZONE PATTERN (10" DIAMETER)

FIGURE 22

3.2.5.2 Uniformity

The width of the etched zones varied from a minimum of about 40% of the zone period near the bottom of the mirror to a maximum of about 80% of the zone period in a small region near the top.

The main cause of non-uniformity was variation in the thickness of the photoresist coating. For reasons not yet understood (but perhaps connected with flow in the tank) the dipcoater produced a thicker film at the top than at the bottom. This resulted in underexposure toward the top. In addition, there was a thickening of the coating toward the sides.

At the top and sides where the coating was thickest and the zones the narrowest, there were regions where the spray development process failed to remove all of the material in the unexposed zones. One such region extended within the 10" diameter field shown in Figures 23 through 30 and may be seen along the right edge.

The development process left a certain amount of debris. As can be seen in Figures 21 and 22, the debris increases as the zones become narrower.

The central obstruction in Figures 23 through 30 was due to the lens and compensator assembly in the holographic setup. The two diagonal marks are from wire stabilizers in this assembly.

3.2.5.3 Repeatability

Several attempts were made to obtain a second zone pattern of a quality equal to or better than that shown in Figures 21 through 30. While by no means discouraging, the results were all less uniform.

The two largest variables were fringe stability and development. Because of the large scale of the holographic setup, the somewhat variable thermal environment, the small tolerance to fringe motion, and the length of the exposures, fringe stability was often marginal. Spray development was done by hand which contributed a further variable.

To produce zone patterns routinely, it would be necessary to closely regulate the thermal environment of the holographic setup and to automate the development process. For optimum quality, it would also be necessary to vary the dip rate in such a way as to cancel out the vertical wedge in the photoresist coating.

3.3 Performance of the Monitor

The main experimental questions to be answered were:

(a) How convenient is alignment of the telescope by the zone pattern method?

(b) How faint may the zone pattern be and still suffice to give fringes of suitable quality?

Sensitivity of the fringes to motion of the mirror surface was not a subject of investigation, there being little question but that the pattern shifts by one fringe wherever the path length is changed by one wavelength.

3.3.1 Adjustment Characteristics

With the aid of the zone plate monitor, alignment and focusing of the telescope proved to be utterly simple. Coarse focusing was done by sliding the primary mirror axially until the diffracted light was brought to a sharp focus on the screen in Figure 14 . Coarse alignment was done by tilting the mirror until the diffracted light returned through the hole in the screen. Fringes were then clearly visible across the face of the primary mirror. Any given fringe pattern could be easily reproduced with the fine controls. In a dark room, a .01% return of the light was quite sufficient for visual alignment if the mirrors were initially not too far from their nominal positions.

3.3.1.1 Fringe Patterns

3.3.1.1.1 Tilt

Figures 23 and 24 show the effects of misalignment about the horizontal and vertical axes respectively. Curvature of the fringes is caused by spherical aberration. Part is due to the use of spherical mirrors in the telescope, part is due to the compromise geometry used in generating the zone pattern (see Section 2.4.2), but most is due to errors in the focal distances αF & βF (see Figure 18) during generation of the zone pattern.

3.3.1.1.2 Defocusing

Figures 25 and 26 show the effect of inward and outward defocusing respectively. Some astigmatism is apparent also. This is due partly to lateral misalignment of the foci during generation of the zone pattern (see Figure 18), and partly to an astigmatizer used to improve the circularity of the laser output beam. This astigmatism is most apparent in Photograph 27, taken in the neighborhood of optimum focus.

3.3.1.1.3 Distortion

The mirror itself was too rigid to allow any appreciable distortion. The wave-front was therefore distorted (by transmission through mylar) to simulate errors such as might occur in a much larger and more flexible mirror. This is shown in Figure 28.

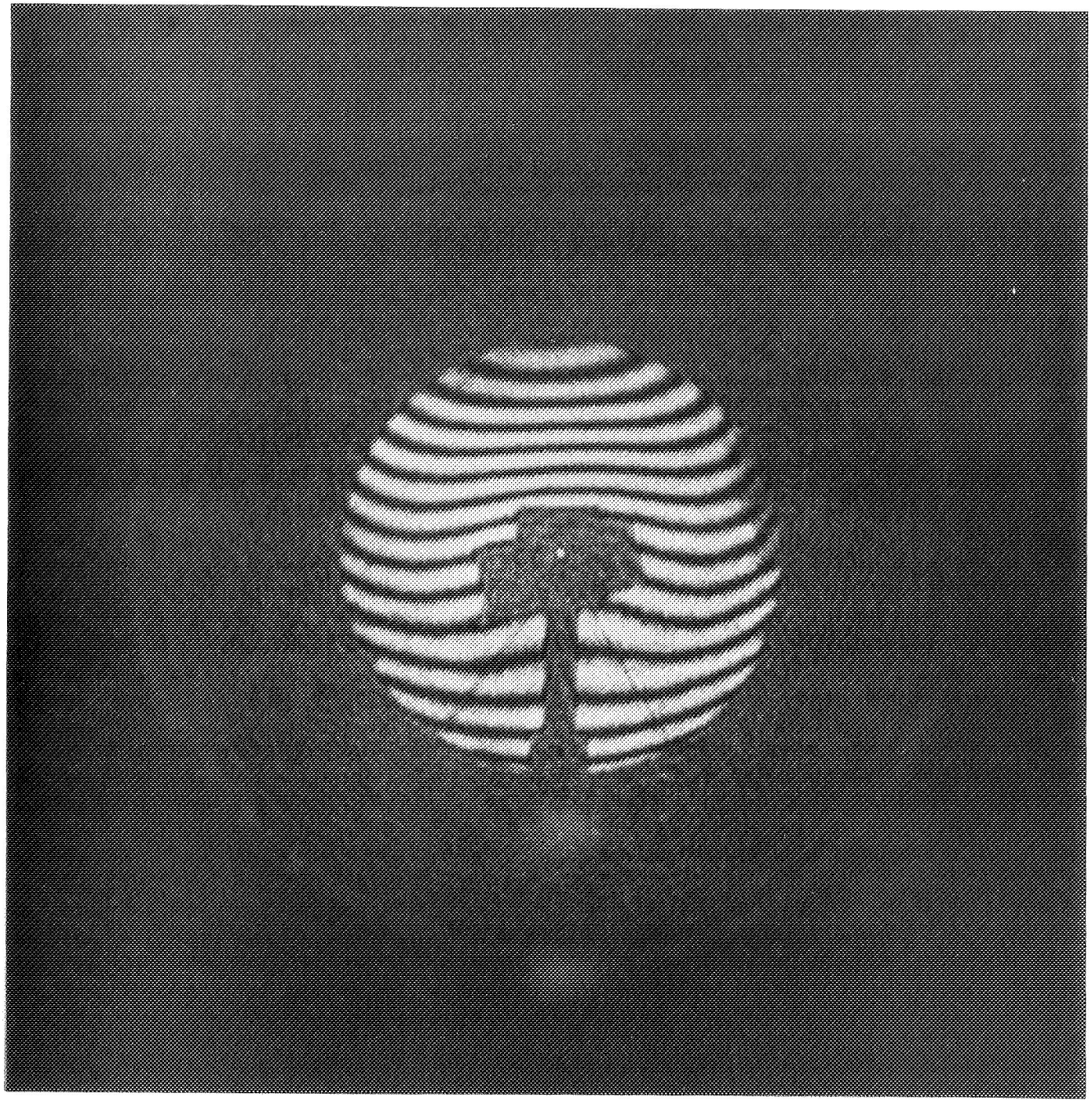

VERTICAL TILT

FIGURE 23

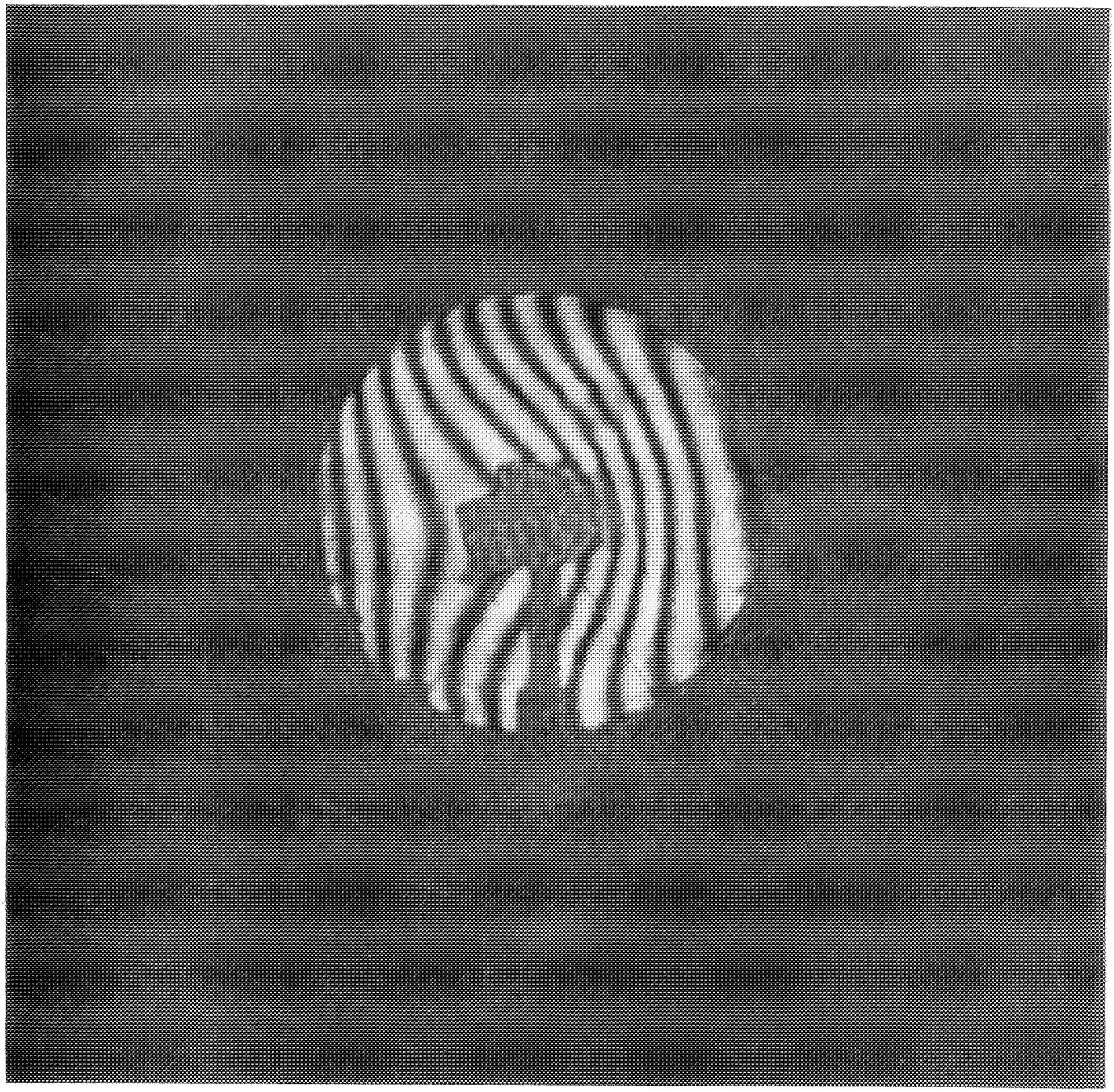

HORIZONTAL TILT

FIGURE 24

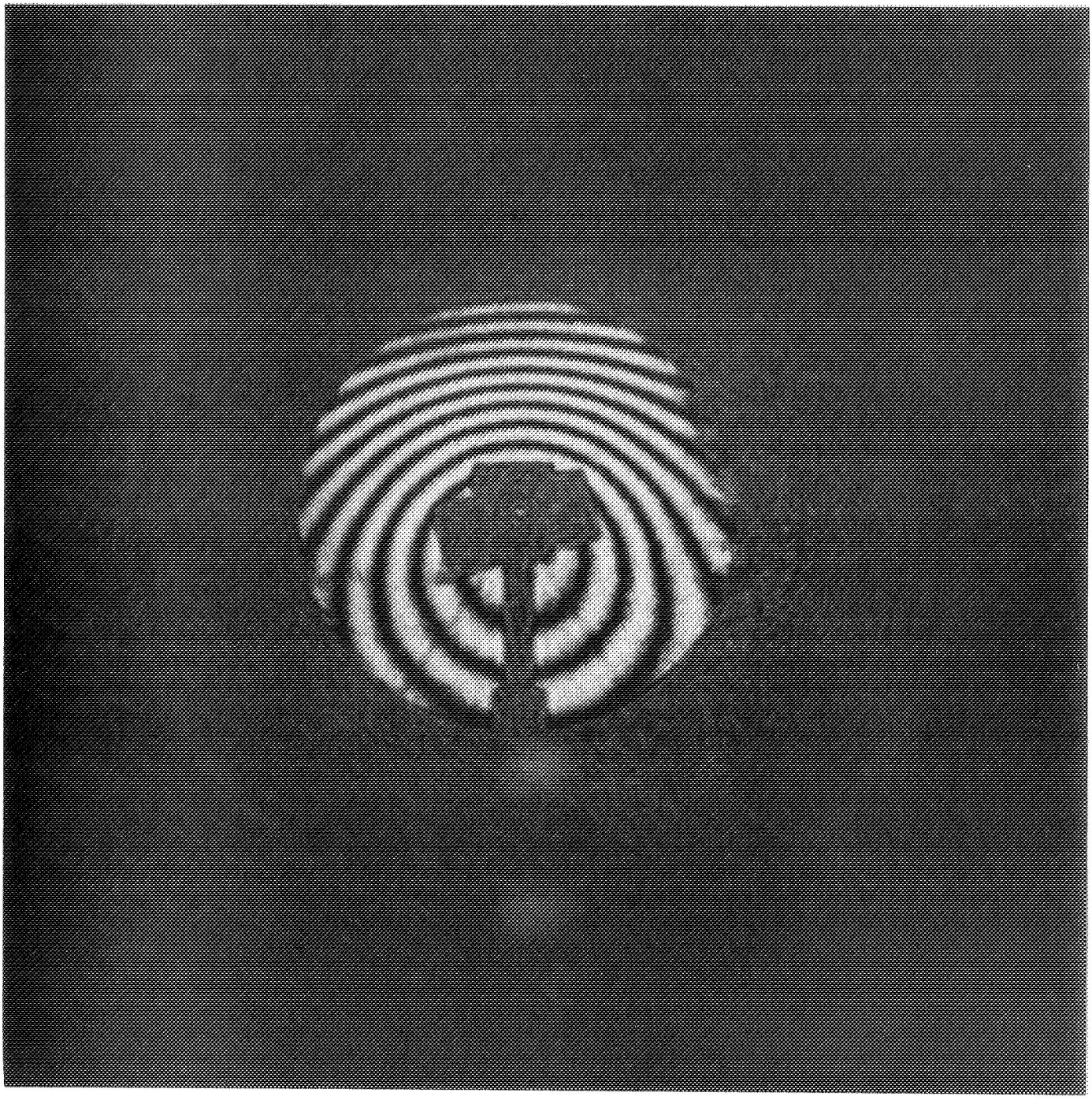

DEFOCUSED (INWARD)

FIGURE 25

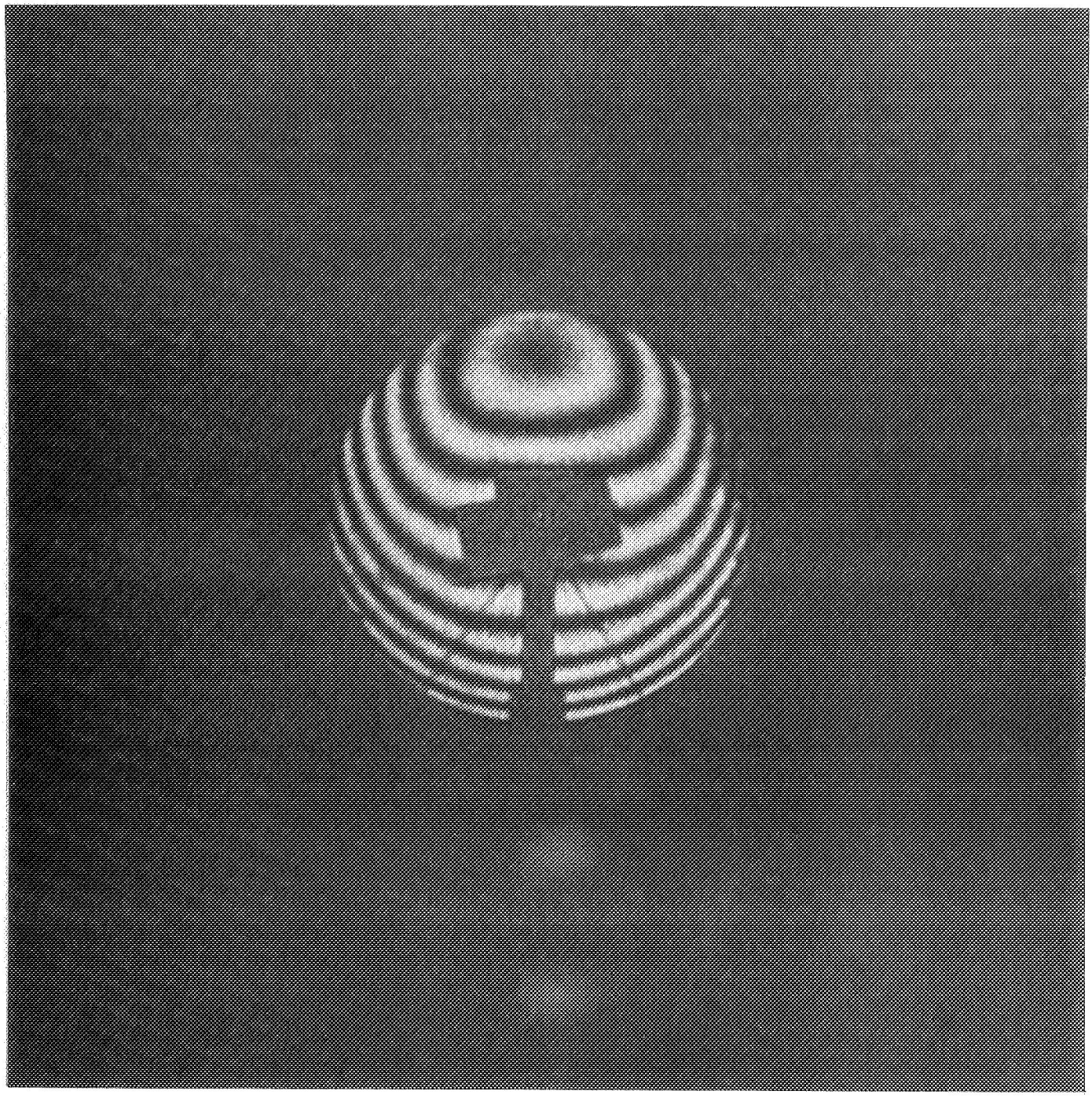

DEFOCUSED (OUTWARD)

FIGURE 26

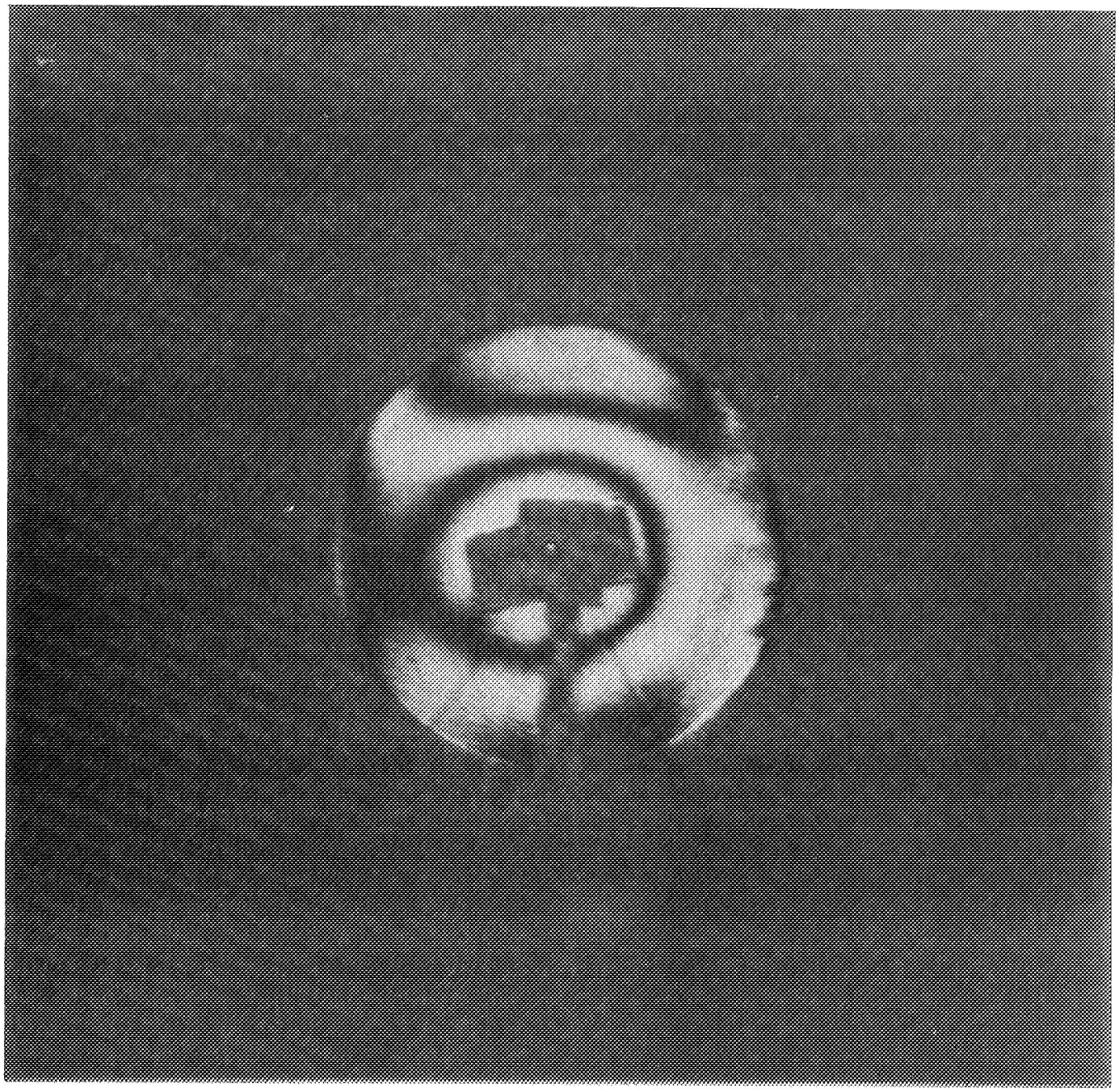

OPTIMUM FOCUS

FIGURE 27

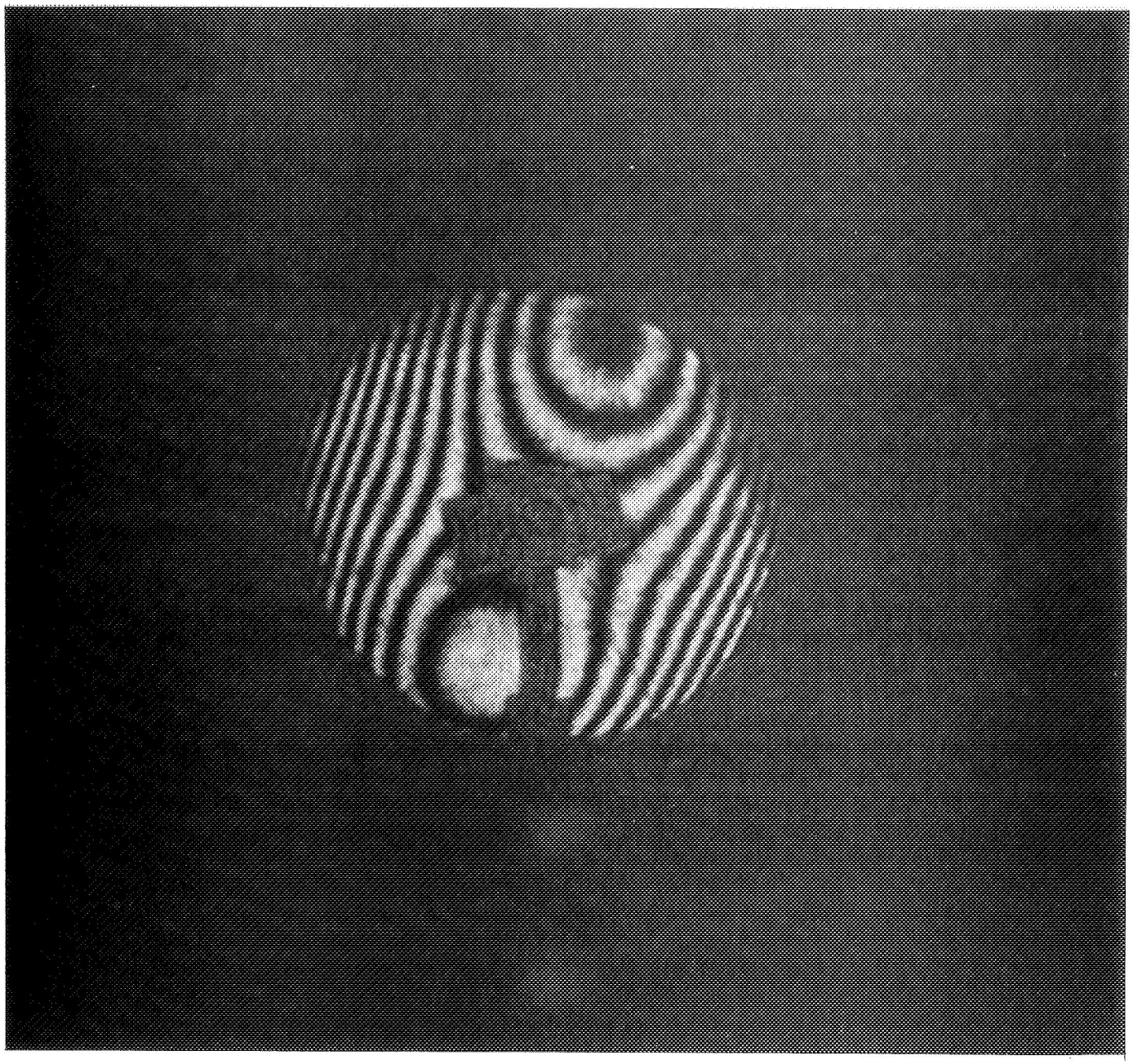

DISTORTION

FIGURE 28

3.3.2 Intensity Characteristics

It was of particular interest to determine how weak the monitoring beam might be and still suffice to give fringes of adequate quality for monitoring purposes.

Fringe quality depends upon the degree to which stray light can be suppressed. To simulate realistic conditions no special precaution was taken in regard to the polish or the coating of the optics. Cleaning was done with "Q-tips" and acetone. The stops were blackened with electrical tape.

Fringe quality is degraded also by diffraction patterns from dust and scratches. This, however, is largely independent of the optical efficiency of the interferometer because these extraneous diffraction patterns are attenuated in much the same way as the principal interference pattern.

To simulate a zone pattern of low efficiency, the monitoring beam was attenuated by two external reflections at 45° incidence from an uncoated mirror (index n=1.51) as shown in Figure 12. A wide variation in intensity was obtained by rotating the plane of polarization of the laser so as to select a reflectivity of $R_{\perp} = .093$ or $R_{//} = .0087$. The reference beam was similarly attenuated.

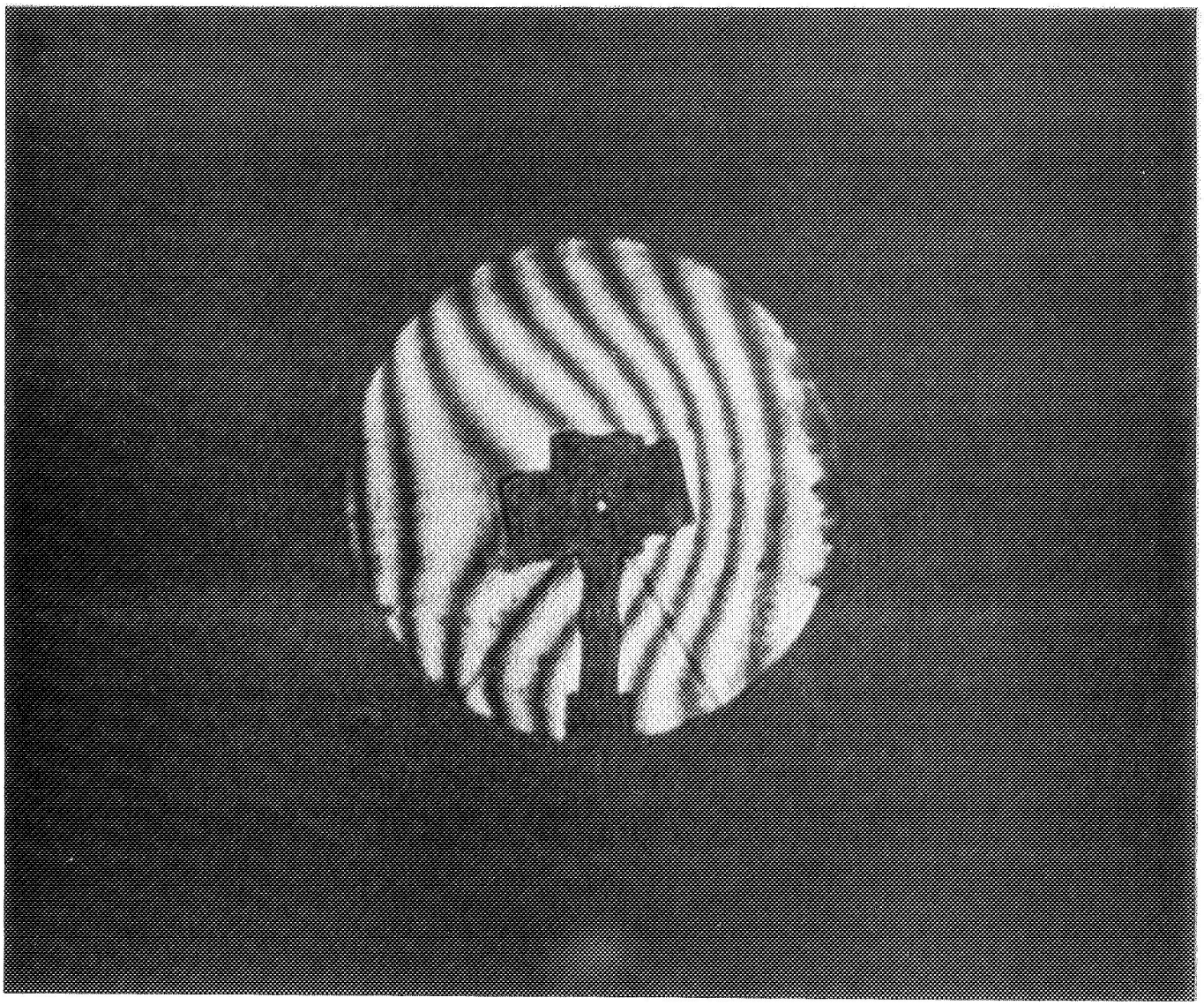

FRINGE QUALITY AT AN ATTENUATION OF .36%

FIGURE 29

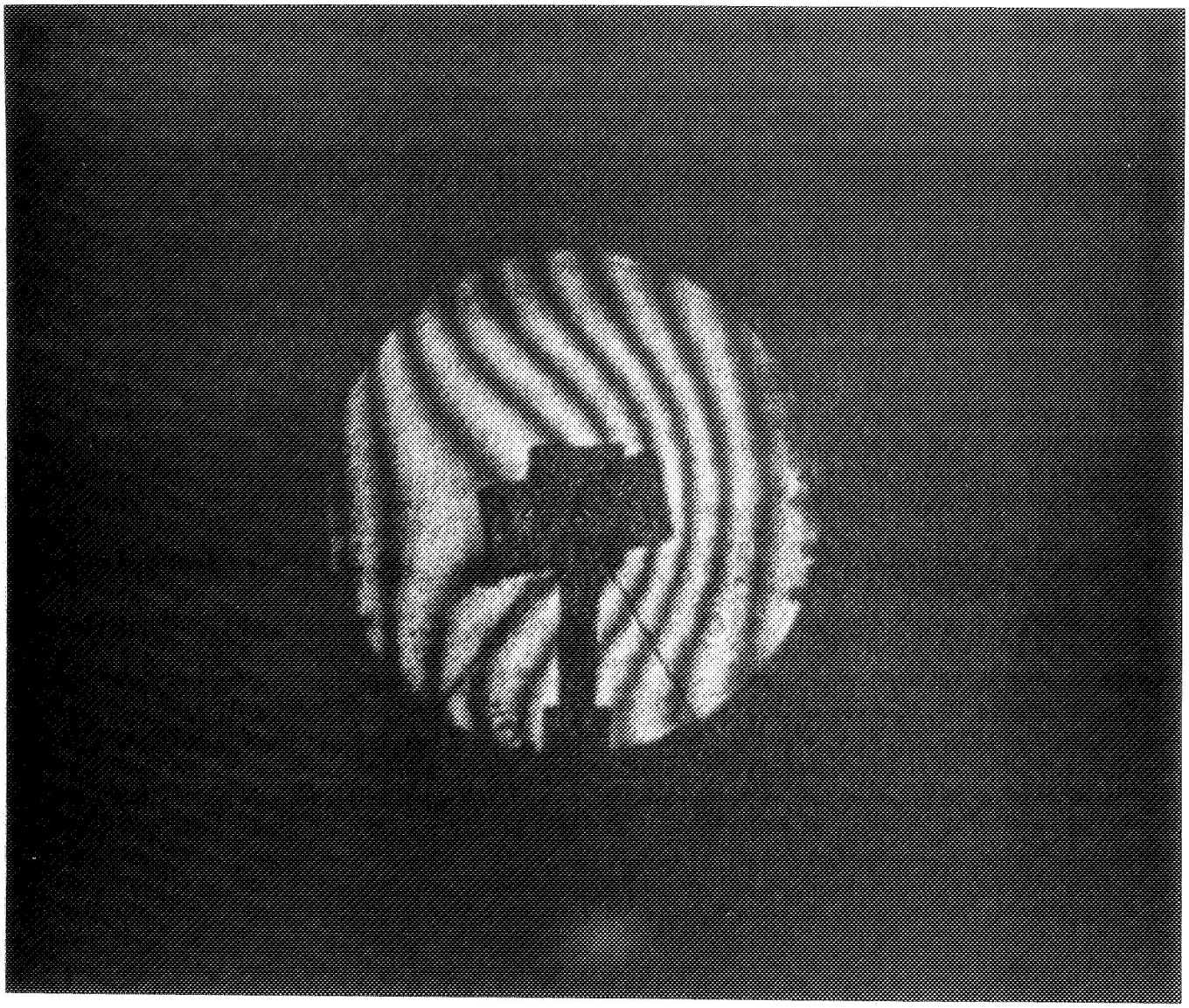

FRINGE QUALITY AT AN ATTENUATION OF .0031%

FIGURE 30

The effect of attenuation on fringe quality can be judged from Figures 29 and 30. The attenuation factors for the monitoring beam in the two cases were:

$$\epsilon_{\perp} < .36\%$$

$$\epsilon_{\parallel} < .0031\%$$

The above attenuation values are conservative since they include a diffraction efficiency factor for the zone pattern of $\frac{4}{\pi^2}$ which is the theoretical maximum. It appears evident that there should be no particular difficulty in obtaining fringes of satisfactory quality at a diffraction efficiency well below .03%.

Figures 22 through 28 were photographed at an attenuation factor below .15%.

4. CONCLUSION

A procedure has been developed for holographically generating f/5 zone plates approaching 12" in diameter. Using this procedure, the zone pattern method of monitoring telescope performance has been demonstrated on a cassegranian telescope with a 12" diameter f/5 primary mirror.

Convenience of the Zone Pattern Method:

The most significant experimental finding is that the primary mirror can be aligned with extreme ease by the zone pattern method. For initial checkout of a large telescope, especially one with a convex secondary mirror, the zone pattern method might well be applied to the secondary mirror, too.

Accuracy of the Zone Pattern Method

The zone pattern method is practical only if:

(a) a suitably stable mirror material is available,

(b) the zones can be generated (or mapped) with suitable accuracy.

Analysis indicates that the thermal stability of materials such as Cer-Vit(R), Zerodur(R) and ULE Quartz(R) is compatible with a $\frac{\lambda_o}{50}$ rms measurement tolerance on the figure of the primary mirror. More experience is required, however, with very large blanks of these materials before the effects of long term creepage can be assessed.

Analysis indicates also that measurement of zone radii to fringecounter accuracy should suffice for calibration of the monitor to an r.m.s. accuracy of $\frac{\lambda_o}{50}$ in the mirror figure. Further study is required, however, to determine the practical accuracy to be expected of an interferometrically controlled machine specially designed for generating (or mapping) the zones.

(R) "Cer-Vit", "Zerodur" and "ULE Quartz" are registered trade names of materials supplied respectively by Owens-Illinois, Schott and Corning.

Effect on Stellar Images

How weak the zone pattern may be and still suffice for monitoring purposes depends upon:

(a) The practical limit to which stray light in the monitor can be suppressed.

(b) The practical limit on the sensitivity of the sensor system used in the monitor.

On both these counts it is reasonably clear that a diffraction efficiency, ϵ_N, as low as .03% will suffice. At this efficiency, diffraction of starlight from the zone pattern will not obscure stars fainter than approximately magnitude 28. Loss in image intensity from diffraction will be below 3% and there will be no appreciable effect on image resolution.

Generation of the Zone Pattern:

The results obtained photographically over a 12", f/5 aperture were unexpectedly good. For checkout of a telescope 3 m in diameter, however, it appears more suitable to generate the pattern with a laser "stylus" under interferometric control.